TECHNICAL REPORT No. 1837
FINAL REPORT

N90 70865

ORI
Silver Spring, Maryland 20910

ANALYSIS OF CONTAMINATION EFFECTS ON CRITICAL SURFACES OF SPACEBORNE PAYLOADS

JANUARY 1981

PREPARED UNDER CONTRACT No. NAS5-25607, MOD 25
FOR
NATIONAL AERONAUTICS AND SPACE ADMINISTRATION
GODDARD SPACE FLIGHT CENTER
GREENBELT, MARYLAND 20771

TABLE OF CONTENTS

LIST OF FIGURES

LIST OF TABLES

I. INTRODUCTION

1.1 SCOPE OF STUDY

The principal goal of this study is to develop a set of contamination criteria for spacecraft by which levels of contamination may be related to specific degradations in the performance of spacecraft. Contamination-induced degradations, as defined in this study, are any detrimental effects produced by the accretion or impact of materials on externally-exposed surfaces.

Spurious signals may also be produced by contaminants in space which emit or reflect radiation into the field-of-view of a sensor. They are transient in nature and will not be classified as degradations. If the source of these contaminants is known, the spurious signals will not be mistaken for natural events. Radiation damage and internal contamination mechanisms are also excluded from the scope of this effort; they will be addressed only if they are relevant to accretion or impact problems.

In the past, contamination of the earth orbital environment has been addressed primarily in mission-specific terms. Major sources of contamination within a mission such as propellent firings, outgassing, and fluid dumps were evaluated for their deleterious impact upon instrument and support hardware systems within the payload or mission of their origin. For example, the CAMEO, a chemical release experiment which was "piggybacked" on the upper stage of the Nimbus 7 launch vehicle, was analyzed to insure that its reaction

products would not contaminate the Nimbus 7 payload sensors nor harm the solar panels. It was shown that the levels of contamination produced by the CAMEO would be insignificant in comparison to those produced by natural environmental effects, including those of the residual upper atmospheric constituents and the micrometeoroid flux.[1,2] It was further shown that contamination levels produced by the CAMEO were small in comparison to those produced during instrument handling, integration, and testing in the best available clean room environment.[3]

Criteria for contamination emitters have been formulated on a mission-specific basis in the past. Standards have been written to forbid the use of exposed surfaces with bad outgassing properties, to define maximum allowable sizes and numbers of particles within the field-of-view of sensors, etc. In most cases, the supporting rationale for the quantitative values has not been documented.

Solid fuel upper stage rocket motors and chemical release modules (CRMs) are two classes of contamination emitters whose deleterious effect upon other spacecraft must be addressed. Time and space windows must be determined for each mission so that no other spaceborne payload is damaged. On the other hand, the criteria for such ignitions must not be drawn in an unrealistically stringent fashion. It is important to realize that other mission characteristics already impose severe constraints upon the firing of both upper stage rocket motors and CRMs. The rocket motor firings are constrained by the orbital parameters of the low-earth parking orbit of the spacecraft and by those of the transfer orbit into which it must be inserted. The ignition of a CRM is constrained to occur in local twilight, within the observational envelope of one or more appropriate ground observatories, and with good atmospheric visibility beneath.[2]

The purpose of this study is to define contamination criteria which are valid on a general basis. In other words, we wish to establish guidelines by which an "acceptable" level of contamination may be defined based upon a minimum number of mission-specific assumptions.

1.2 METHOD OF APPROACH

1.2.1 Data Base Development

The development of generalized contamination criteria is a multi-faceted problem. Due to the very nature of this problem, no simple tabulation of contaminant species, contamination prone surfaces, or case histories of performance degradations produced by contamination can be made "all-inclusive." ORI has therefore approached the problem in a generic manner. The first phase of ORI's effort involved a survey of case histories of performance degradations in space for which contamination was the known or suspected cause. ORI has surveyed published documents on contamination-induced problems, has interviewed numerous scientific and engineering personnel, and has summarized and analyzed the results of this survey. Based upon this data survey and the subsequent analysis, we must report that data from spaceborne experiments do not contain sufficient information to permit the formulation of these relationships. In most cases, even the species of the major contaminant cannot be unambiguously defined.

The survey of contamination problems provided a useful guideline to identify some of the contamination-prone subsystems which are treated in this study. It was also important because past failures and degradations of spaceborne payloads had often provided the impetus for theoretical analysis and for earth-based experiments aimed at understanding the contamination mechanism and eliminating it on subsequent missions.

There is a substantial collection of ground-based experimental data taken under conditions which strongly resemble those found in space. In most cases, contaminant species can be identified and quantified and the physics of the degradation mechanism is well understood. Because of this finding, ORI de-emphasized the study of space experiments and directed the bulk of the remaining effort to the classification of laboratory data and to the formulation of quantitative relationships between the levels and species of contamination and the degradation of critical surface parameters.

ORI also surveyed experimental and theoretical estimates of the earth orbit environment, including the micrometeoroid flux and the distribution of residual atmospheric constituents. Most of the experimental data on micrometeoroids have been taken from specimens which were exposed to the ambient environment on manned space missions and were subsequently returned to earth for analysis. The information which ORI has compiled on spaceborne contamination effects, on ground-based contamination experiments, and on natural environmental contaminant fluxes is summarized in Chapter II of this report.

1.2.2 Formulation of Criteria

In order to formulate these relationships with a minimum number of specific assumptions about individual instruments and contaminants, ORI has adopted the following approach:

1. Generic classes of contamination-prone instruments and support subsystems are identified.

2. Critical surfaces of these instruments are specified and their important parameters are listed.

3. Degradations of these critical properties by various contamination mechanisms and by manufacturing error budgets are compared in simple but quantitative models.

4. Worst case contamination receivers are identified.

5. Acceptable levels of anthropogenic contamination in space are defined to be those whose effects are insignificant in comparison to degradations produced by the natural space environment or by state-of-the-art component manufacturing tolerances.

1.2.3 Classification of Surfaces

Chapter III contains an outline by which critical surfaces may be identified and classified. ORI has utilized a generic approach by establishing broad classes of contamination receivers, i.e., those surfaces whose critical properties can be adversely affected by contamination. The list of contamination receivers includes, of course, all surface types which were found to be contamination-prone in the analysis of previous performance degradations. It also includes those surfaces which have a potential for contamination sensitivity as judged from the analysis of ground-based laboratory data or from the stringent specification on a surface property which results from a systems analysis. The surfaces are then classified according to several key parameters:

1. Location
2. Typical Application
3. Spectral Range
4. Critical Property
5. Operating Temperature
6. Typical Surface

Chapter IV identifies those surface parameters which are most prone to contamination-induced degradations and develops models which permit the quantitative comparison of different mechanisms which degrade that same parameter. For example, the total integrated scatter (TIS) is used as an index of stray light scattering. Its value is calculated for several mechanisms, including reflective and dielectric particulate accretion, cratering by micrometeoroid impact and accretion of an irregular molecular film.

Chapter V employs the models developed in Chapter IV, micrometeoroid flux data from Chapter II, and estimates of manufacturing tolerances in surface quality to perform quantitative comparisons of surface degradations. Worst case contamination receivers are identified by a process of elimination. Limits are then established and permissable levels of contamination are defined.

Chapter VI presents ORI's conclusions and recommendations for further study.

Table 1-1 is a flow chart which summarizes ORI's technical approach to the definition of contamination criteria.

1.3 REFERENCES

1. Dubin, M., "The CAMEO Experiment and Possible Interaction With the Nimbus-G Spacecraft," Internal NASA/GSFC Memorandum, (June 13, 1978).

2. Chemical Payload for the Delta Launch Vehicle, Thiokol Corp., Ogden, Utah (Feb. 1977), pp. 73-80.

3. Compatibility of CAMEO Auxiliary Payload and the Nimbus-G Mission, Technical Report 1213, ORI, Inc., Silver Spring, MD, (Sept. 1977), pp. 5-2.

TABLE 1.1

CONTAMINATION STUDY FLOW CHART

TASK	SUBTASKS
Identify contamination-prone instruments and support subsystems and the natural degradations to which they are exposed in space.	• Analyze history of contamination problems and experiments in space • Quantify natural background fluxes of contaminants • Analyze ground-based experiments which simulated the space environment
Catalog general classes of contamination-prone surfaces and identify their key parameters.	• Define general classes of instruments based upon critical surfaces parameters • Tabulate surface properties
Develop models which permit comparison of different contamination and error budget effects.	• Identify relationships between critical surface parameters and surface defects • Develop analytic models to relate surface degradations to levels of contamination and other defects.
Identify "acceptable" levels of contamination.	• Calculate degradation in surface parameters as a function of contamination levels • Calculate or estimate degradations in surface parameters produced by the natural environment, by manufacturing errors, and by the handling and deployment environments. • Identify worst case contamination receiver • Compare the above effects and identify as negligible those contamination effects which are sufficiently small with respect to those produced by the environment or by manufacturing errors.
Summarize conclusions and make recommendation for further study.	

II. CASE HISTORIES OF CONTAMINATION-INDUCED PERFORMANCE DEGRADATIONS IN SPACE

2.1 OVERVIEW

This chapter presents an overview of several types of contamination-related problems which have occurred or have been suspected in space missions. This set of case histories is not intended to serve as a catalog of all known cases of contamination; it focuses instead upon several generic classes of contamination and documents information which is available about them. Data on the background flux of micrometeoroids are also summarized.

2.2 CONTAMINATION OF RADIANT COOLERS AND ATTACHED OPTICS

Radiant coolers have been used on a large number of spaceborne missions to provide passive cooling of small thermal loads to the 80-120 K range. These loads are generally in the milliwatt range and are typically produced by cold focal plane assemblies consisting of infrared detector arrays, filters, and possibly preamplifiers. A radiant cooler consists of a highly emissive "cold patch" which is thermally coupled to the focal plane assembly and thermally isolated from the remainder of the spacecraft. It is oriented to view "deep space" and surrounded by a shield with specular inner surfaces to protect it from radiation from the sun, the earth, and the spacecraft. The shield is also thermally isolated from the spacecraft and therefore operates below ambient temperature.

Radiant coolers have frequently exhibited a gradual degradation in performance which was produced by a rise in the temperature of the focal plane assembly and/or a higher background noise level in the infrared channel. In most cases, this degradation could be reversed by interrupting the data gathering and baking out the cooler. The bake-out process may be accomplished by using heaters or by re-orienting the spacecraft attitude so that the cooler faces the sun. Figure 2-1 illustrates the loss of sensitivity experienced by the radiant cooler of the Heat Capacity Mapping Radiometer (HCMR) which is currently being flown onboard the Application Explorer Mission (AEM) satellite which was launched in April 1978. The infrared channel sensitivity degraded gradually but returned to its original value after a period in which the cooler door was closed and the temperature was allowed to exceed 200 K. When the data taking was resumed, degradation began again, although at a slower rate. It is believed that water vapor condensation was responsible for this problem.[1]

The HEAO-B mission also experienced a problem in which a cryogenic optical instrument lost transmissivity. A heater was turned on to bake out the instrument and it temporarily alleviated the problem. Based on this evidence and on the fact that the cooler and optical assembly had the same vacuum system, it was postulated that water vapor was outgassed from the multi-layer insulation and condensed on the optical surfaces.[2]

Several other degradations of radiant coolers on NASA/GSFC spacecraft have been documented:[3]

- A Very High Resolution Radiometer (VHRR) onboard the Improved Tiros Operational Satellite (ITOS) also experienced a thermal degradation which was reversible upon heating of the radiant cooler and for which condensation of water vapor was the suspected mechanism.

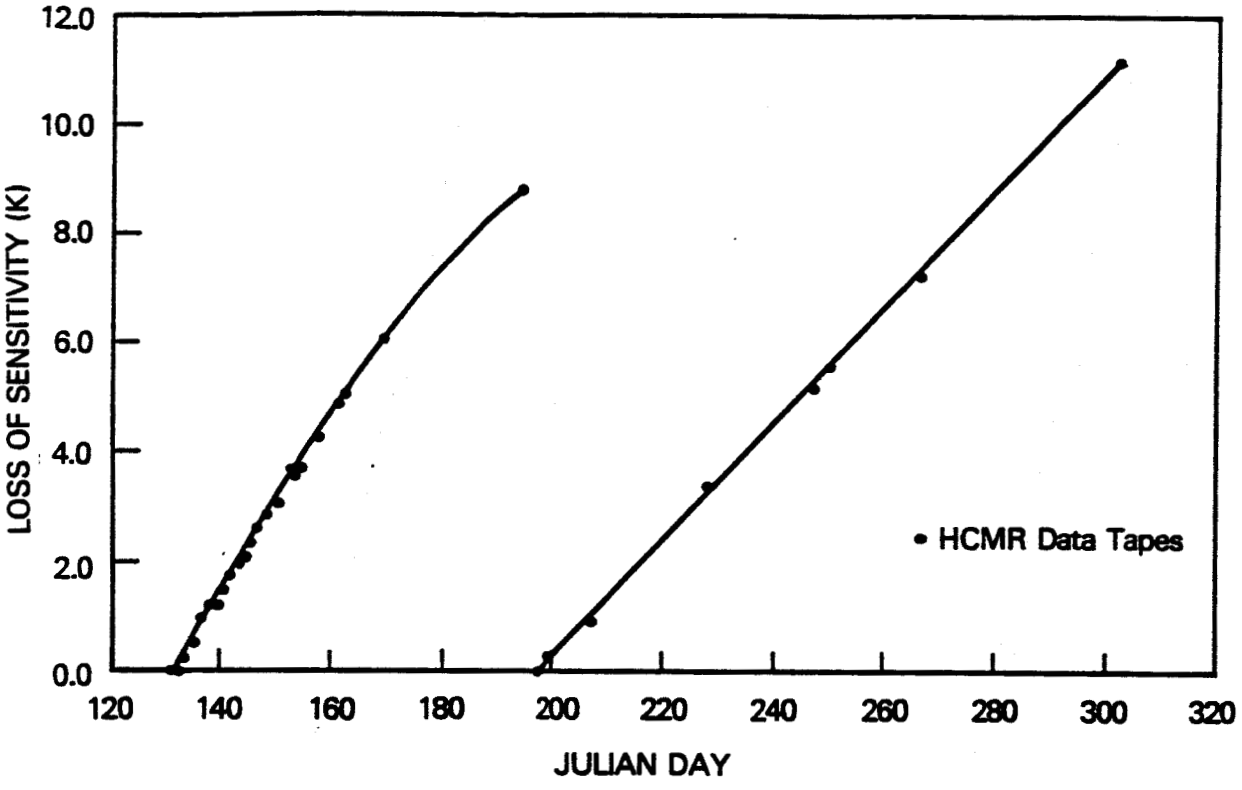

FIGURE 2-1. HCMR LOSS IN SENSITIVITY VS JULIAN DAY

- The SCMR, which was flown aboard Nimbus-1, had a two-staged radiant cooler with a cold patch operating at 115.7 K and a first stage cone at 172 K. The cone temperature was approximately 10 K warmer than predicted. The cold patch experienced a reversible degradation of about 1 K. The higher temperature of the cone was attributed to poorer-than-expected insulating properties of the multi-layer insulation and to possible contamination of the cone surfaces during testing.

- The Defense Meteorological Satellite Program (DMSP) has involved the launch of 8 satellites to date. One of the payload instruments, the WHR, produces high-resolution cloud cover maps of the earth's surface. The WHR has a thermal channel which uses a two-staged A. D. Little radiant cooler, shown in Figure 2-2.

The first DMSP radiant cooler experiment was flown in 1972 on the Block 5B-2 Satellite and contained the radiant cooler only. It was used as a proof-of-principle experiment to establish the refrigerating power and the thermal stability of the radiant cooler. The Block 5B-3 satellite, launched later in 1972, contained a WHR with an 8.9-13 μm channel. This channel utilized an infrared detector with an operating temperature of 110.5 K. A gradual degradation, which was detected by rising cone temperature and decreasing patch control power demand, began almost immediately. After nine weeks of operation, the channel sensitivity had decreased by 50 percent. Use of heaters restored the cooler parameters to their initial value but returned the channel sensitivity to only 75 percent of its original value. A subsequent bake-out after 15 weeks of operation, again restored the cooler performance but was unable to improve the channel sensitivity to a value significantly over 50 percent. A similar WHR was flown on the Block 5B-4 satellite in 1973. The outer stages of the radiant cooler were not heated during this mission and the channel sensitivity had decayed to 40 percent of its initial value after 3000 orbits.

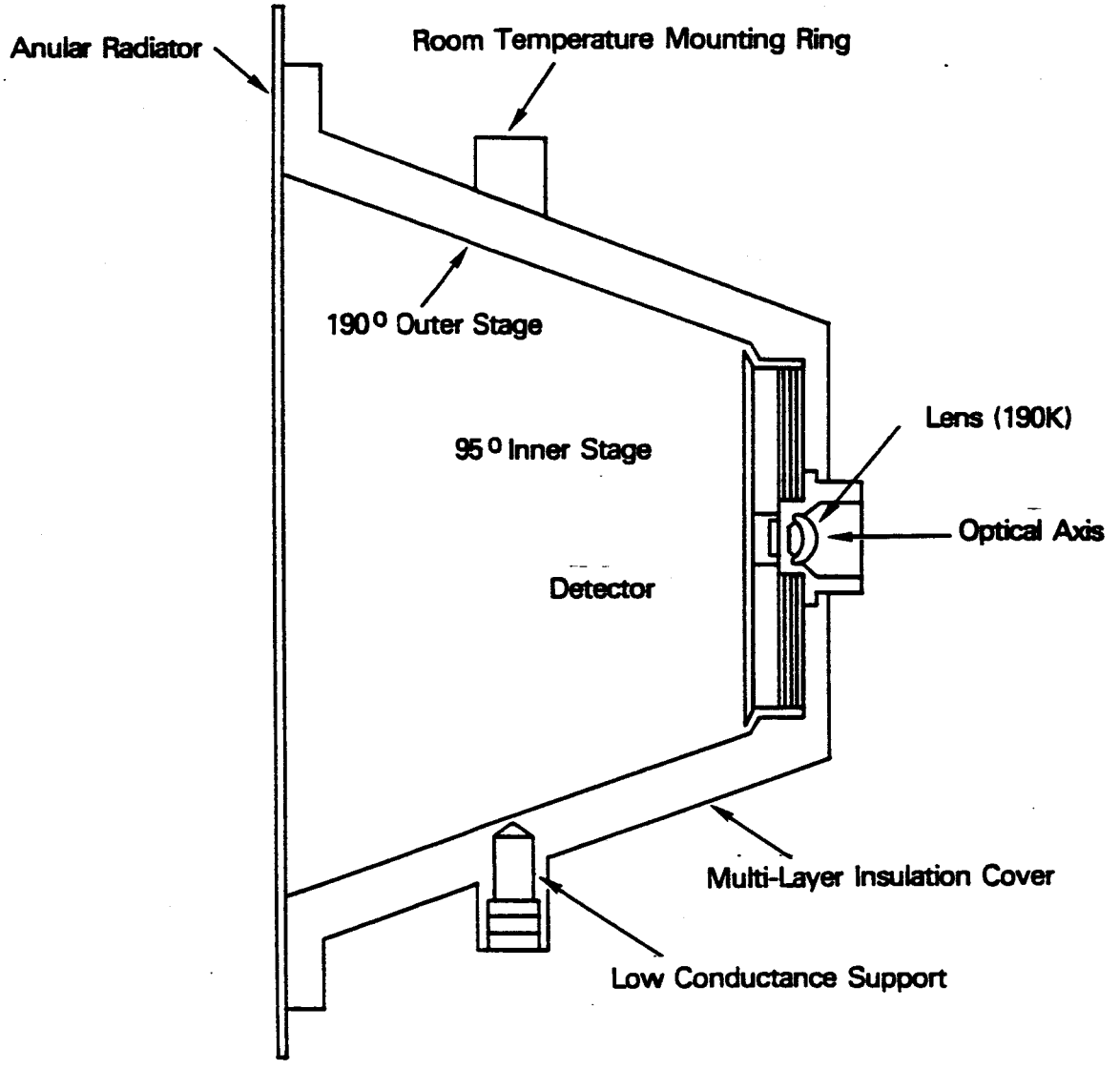

FIGURE 2-2. RADIANT COOLER - TWO STAGE CONE DESIGN - (A. D. LITTLE DESIGN)

Two additional WHRs were flown onboard the Block 5B-5 and Block 5B-6 satellites which were launched in 1974. The thermal infrared channels on these systems were modified to include a warm window between the warm portions of the sensor and the refrigerated singlet lens on the cold assembly. The use of these warm windows greatly reduced the degradation problem.[4,5]

In summation, surfaces which operate significantly below ambient temperature have a recurring history of contamination induced degradation. Water vapor condensation is suspected as the primary contaminant for the following reasons:[2,6,7]

1. Water is known to outgas from multi-layer insulation.

2. The time-dependent restoration of performance upon heating follows the profile which is typical of water vapor.

3. In one instance, a spectrometer became contaminated and exhibited water absorption bands in its spectrum.

The exact mechanism of degradation is unknown. Because the temperature of the cone was found to increase, it may be concluded that its specular inner surface experienced an increased emissivity. It is therefore also probable that the specularity of the surface decreased as well, causing an increased flux of diffusely-scattered sunshine, earthshine, and/or spacecraft radiation to impinge upon the cold patch. The emissivity of the cold patch could also increase.

The degradation of the cold optical surfaces, unlike that of the radiant coolers, was not completely reversible upon bakeout. Possible mechanisms for this effect include reaction of water with a hygroscopic lens overcoat and deposition of trace amounts of non-volatile contaminants. Quantitative relationships between levels of contamination and levels of performance degradation cannot be established from the available data.

2.3 PARTICULATE CONTAMINATION OF OPTICAL SENSORS

Particulate contamination can produce degradation in the performance of optical sensors by a number of mechanisms. Low-velocity particles can accrete on a surface and cause an increase in the level of stray light scattering. High velocity particulates which impact surfaces directly can diminish both their throughput and their ability to image. Indirect impacts of high velocity micrometeroids or particulates may also create a problem by causing small pieces of spacecraft material to break loose from the surface. These particulates may then either adhere to a critical optical surface or drift through the sensor's field of view.

The following summary of several case histories provides examples of degradations for which each of the above-mentioned mechanisms were the confirmed or suspected cause.

2.3.1 Skylab Solar Coronagraph Experiment

A solar coronagraph is strongly degraded by stray light scattering because of the small angular separation between the relatively weak corona and the much more luminous photosphere. As a consequence, a solar coronagraph is extremely sensitive to contamination of either its optical surfaces or the optical path within its field of view. The planning of the Skylab mission included careful attention to the problem of contamination minimization with the coronagraph experiment as a driving requirement. At the Skylab altitude of 430 km, molecular contaminants from the spacecraft were swept away almost immediately and did not have any significant impact on the experiment. Water in the form of ice crystals was the major contaminant. The average rate of water loss from Skylab was estimated at about 5-1/2 kilograms per day.

The outer occulting disk of the coronagraph was cleaned by the astronauts during their EVA. The deleterious effects of accreted contaminants were less noticeable than those of free-floating particles within the field-of-view.[8]

2.3.2 Contamination Monitor Experiment

The AIMP-D was one of a series of lunar orbiting satellites. It experienced overheating (60 C) which contributed to its battery failure when the orientation of one of its surfaces remained nearly perpendicular to the sun line for an extended period of time. A subsequent analysis indicated that a doubling of the solar absorptance of this surface, induced by contamination, was the only logical explanation. The fourth stage rocket motor, which was mounted directly to spacecraft, was the suspected source of this contamination.

The next spacecraft in this series, AIMP-E, was redesigned to reduce the effect of changes in the solar absorptance of this surface. A Contamination Monitor Experiment was also included on this satellite. The monitor measured the reflectance of a polished aluminum surface by using a tungsten filament lamp as the source and a solar cell as the detector. A sealed reference cell was used for calibration. The spectral response of this system was greatest at approximately 900 nm.

The AIMP-E was launched on July 19, 1967 and the flight experiment was conducted for about 69 hours: from launch to fourth stage separation. No contamination was detected during launch or during the firings of the first three stages.

The monitor detected the onset of contamination approximately three minutes after the firing of the fourth stage. The absorptance reached its maximum value approximately 18-1/2 minutes after the thruster firing and then declined slightly. The final absorptance was 23.5 percent, more than twice the original value of 10 percent.[9]

2.3.3 Defense Meteorological Satellite System (DMSS) Horizon Sensor Degradation

The Defense Meteorological Satellite System (DMSS) is utilized to provide high resolution cloud cover maps. It contains a nadir viewing sensor

with two visible/near IR channels (400–800 nm and 400–1100 nm) and one thermal IR channel (10.5–12.5 μm). A 1.5–1.64 μm band will be added to future sensors for snow/cloud discrimination.

The DMSS satellite employs thermal IR horizon sensors with germanium lenses. Those forward-looking horizon sensors whose exposed surfaces were oriented into the direction of motion of the satellite have experienced failures, those which had look angles toward the aft direction have not. Because of the directional assymetry, these failures have been attributed to erosion of the lens surface by material bombardment. The source of the erosion (micro-meteoroid, orbiting particulates, return flux, etc.) has not been determined.[4]

2.3.4 Vela Bhangmeter Controversy

On 2 September, 1979, two bhangmeters (light sensors) onboard a Vela surveillance satellite detected a double-peaked pulse of light similar to those produced by a nuclear explosion. To date, there is considerable controversy as to whether a clandestine nuclear weapon detonation did in fact occur. One alternative explanation which has been advanced is that a high velocity micro-meteorioid impact caused low-velocity particles of aluminum, paint, etc., to be ejected from the spacecraft and to pass through the fields-of-view of the bhangmeters. The controversy apparently cannot be resolved based upon spacecraft data alone; much of the debate hinges upon the analysis of potentially corroborative evidence in the form of a concurrent hydro-acoustic signal detected at an undisclosed location or a concurrent traveling ionspheric disturbance detected at the Arecibo-Radio-observatory.[10,11,12]

2.4 LOSS OF THROUGHPUT ON SOLAR-VIEWING OPTICAL SURFACES

Solar viewing places very stringent demands upon optical systems. In the first place, the sun is an extended, high-intensity, low-contrast source of radiation. Because of these characteristics, stray light scattering is a severe problem. Any effect which increases the stray light scattering of an

optical surface exposed to solar radiation will be more apt to diminish the utility of the data than would an equivalent degradation in a stellar telescope.

The high concentration of solar radiation can produce other undesirable effects. The most obvious effect is the heating of surfaces exposed to solar flux. The flux density to which a surface is exposed may be multiplied by concentrating optics. Another important effect is the interaction of high-intensity vacuum ultraviolet radiation with surface coatings and contaminants. This radiation can induce chemical changes in materials which are normally very stable, particularly in organic compounds.

Several case histories, including the history of flights of grazing incidence solar telescopes on sounding rockets, are discussed in the following text.

2.4.1 OSO-8 Mission

OSO-8 is a solar-dedicated free-flying satellite which was launched in 1976. Its payload included two UV/visible telescopes of the Cassegrain configuration. Both of these telescopes were fabricated using materials and techniques which had a previous history of success in stellar astronomy satellite missions. These telescopes had a purge gas system but did not have aperture doors.

Prior to launch, there was severe concern about solar heating effects. The concave primary mirrors of both telescopes produced concentrated fluxes of about 100 solar constants at their respective primary mirrors. Since these telescopes were flown without aperture covers, there was also a possibility that the primary focal point would dwell upon the baffles or the secondary support "spider" during the process of solar acquisition and would overheat their optically-black surface coatings. The acquisition operation was favorable, however, and an overheating of the off-axis components (the baffles and spider) did not occur.[13,14]

After two days of operation, both of these telescopes had experienced a severe loss of optical throughput, particularly at ultraviolet wavelengths. Several mechanisms were suspected of degrading the aluminum-coated, magnesium fluoride overcoated mirror surfaces. The most likely candidates were the production of color centers in the overcoat by radiation and chemical alteration of a previously-transparent film of hydrocarbon contaminant upon exposure to the solar flux.

Subsequent laboratory tests showed that aluminum-coated mirrors with a magnesium fluoride overcoat were degraded by vacuum ultraviolet irradiation (VUV). An Auger spectroscopy experiment which was performed to identify the specific mechanism detected a thin layer of carbon and oxygen at the surface (Hydrogen is not detected in Auger spectroscopy). The degradation mechanism was identified as hydrocarbons deposited on the mirror surface and catalized by heat and/or VUV radiation.[15,16]

2.4.2 Space Flights of Grazing-Incidence Telescopes

A grazing-incidence telescope is usually constructed with one or two extreme off-axis conic section mirrors. These mirrors reflect extreme ultraviolet (EUV) and soft X-ray radiation at angles ranging from a few degrees from the surface to fractions of a degree. (No material reflects radiation of these wavelengths efficiently at normal or near-normal incidence.) A grazing incidence mirror usually has an uncoated reflective surface of a heavy precious metal such as iridium, platinum, or gold which is polished to a very stringent microroughness tolerance (typically 10-30 Angstroms, RMS).

Because of the grazing incidence geometry, the optical path length through a contaminant film is many times greater than the film's thickness. It would therefore appear likely that a small contaminant film would produce a significant performance degradation.

Drs. Werner Neupert and Gabe Epstein, of NASA/GSFC were contacted concerning the contamination sensitivity of grazing incidence telescopes for solar observations. Neither of these scientists had observed a degradation in performance which was attributable to contamination.[17,18] Dr. Neupert has recovered some sounding rocket payloads with "visibly dirty" grazing incidence mirrors without experiencing a lower-than-expected data quality. He offered the following explanations for the apparent contamination insensitivity of the optics:

- All materials, including contaminants, reflect electromagnetic radiation to some extent at grazing incidence
- State-of-the-art grazing incidence telescopes do not approach diffraction-limited performance under ideal conditions.

Mr. John Mangus, of NASA/GSFC, discussed the OSO-7 mission which contained a grazing incidence solar telescope. Intercomparison of spectra taken after one year of deployment has shown that the degradation of the mirrors was negligible. (Some detector degradation did occur during this interval.) The ability of a contaminant to distort the optical path of a high energy photon was a function of the electron density of the contaminant. It is therefore plausible that contaminants of low molecular weight will have relatively little impact upon the properties of the heavy metal surface coating which is utilized in a grazing incidence telescope.

Contamination effects in stellar EUV/Soft X-ray observations will be less critical than in observations of an extended high-intensity source such as the sun.

2.5 SUMMARY TABLE

The preceding information is summarized in Table 2-1.

2.6 BACKGROUND MICROMETEOROID FLUX IN EARTH ORBIT

The background flux of micrometeoroids is one of the components of the natural environment which must be compared to contamination effects.

TABLE 2.1

CONTAMINATION-INDUCED DEGRADATION OF SPACEBORNE SYSTEMS

Receiver Surface	Mission and Instrument	Degradation Mechanism	Suspected Contaminant and Origin	Supporting Experiments	Key Individuals
UV Telescope Optics	Instrument OSO-8 Both Solar Telescopes	Loss of more than two orders of magnitude in optical throughput within one day of solar observation	Hydrocarbons from ground-based handling or outgassed from coating polymerized or otherwise altered by solar UV radiation	Auger Spectroscopy on similar mirror surfaces	Eric Metzger, ORI, Inc. John Osantowski, NASA/GSFC John Oberright, NASA/GSFC
Radiant Cooler mirror surfaces, cold patches, and/or cyrogenic optics	Nimbus III HRIR	Rise in temperature-(reversible by periodically orienting the cooler toward the sun to bake-out contaminants)	Water vapor outgassing from insulation	---	Alan Sherman, NASA/GSFC
	Application Explorer Mission HCMR	Loss of IR channel sensitivity (reversibly by bakeout)	Water vapor	---	W.L. Barnes NASA/GSFC H.C. Price NASA/GSFC
	HEAO-B	Loss of transmissivity by cooled optics (reversible by bakeout)	Water vapor-outgassing from insulation	----	Alan Sherman NASA/GSFC
	ITOS	Radiant Cooler	Water vapor	----	
	VHRR NIMBUS-1 SCMR	Radiant Cooler Mirror cone	Insulation problem and contamination during testing	----	W.L. Barnes NASA/GSFC H.C. Price NASA/GSFC
	Meteorological Satellite Program WHR	Contamination of Radiant Cooler Surfaces (Reversible on heating) and of cold optics (partially reversible, reduced on later missions by warm window)		Monitoring of mirror cone and cold patch temperatures	V. Williams Westinghouse Electric Corp., Baltimore, MD.
Outer occulting disk of solar coronagraph	Skylab Solar Coronograph	Particle Accretion	Contaminants from space craft	Removed by cleaning during Astronaut EVA, some photographs made	J. McGuire NASA/MSFC
Thermal control surface	AIMP-D Space Battery & Power System	Lost power due to loss of thermal control via contamination-induced increase of solar absorptance		See Below	R.N. Sheehy NASA/GSFC
Polished Metal surface	AIMP-E contamination Monitor Experiment	Fourth stage firing increased solar absorptance	Solid rocket combustion products	Lamp and detector measured surface reflectivity	R.N. Sheehy NASA/GSFC
Germanium lens	Defense Meteorological Satellite System-Horizon Sensors	Loss of Resolution	Material bombardment of forward-looking sensors	----	V. Williams Westinghouse Electric Corp., Baltimore, MD.

Impacts of micrometeoroids on spacecraft have been measured using various detectors on the Pioneer 10/11 mission and on the MTS satellites.

Microcraters on lunar surface samples have been analyzed by optical and electron microscopy to deduce dust particle fluxes.[20] Measurements of surfaces which were exposed to space on the S-149 Skylab Experiment provide a direct experimental sample of the microcraters which are formed on an exposed surface in low earth orbit.[21] A standard meteoroid flux model is also given. The experimental data are presented and model parameters are presented in Figure 2-3.

It should be noted that there are significant discrepancies in the data, as great as three orders of magnitude in some instances. In particular, the fluxes deduced from the Skylab microcrater data are greater than those deduced from other measurements. One explanation for this phenomena lies in the fact that the Skylab data were interpreted under the assumption of a crater-to-projectile diameter ratio of three. Other investigators assume that the mass removed from the crater is proportioned to the energy of the incident micrometeoroid and compute a ratio of greater than three for hypervelocity impacts. In all cases, hypervelocity impact craters were found to approximate a hemispherical geometry.[21,22,23]

The greatest difference between the Skylab model and the others is the presence of very high flux levels of 10^{-14} -10^{-15} gram micrometeoroids in the Skylab data. This flux is probably produced by the break-up of larger meteoroids in the near-earth environment.

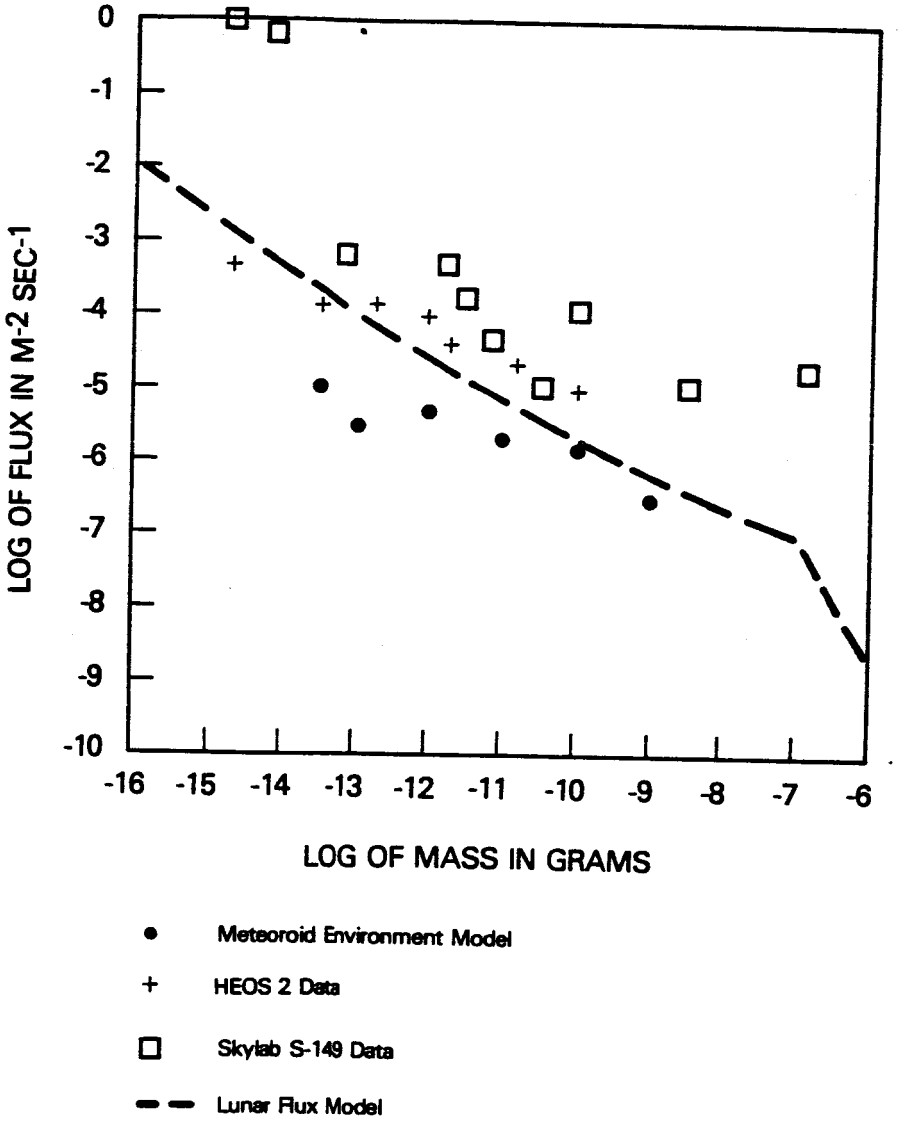

FIGURE 2-3. MICROMETEOROID FLUX LEVELS

2.7 REFERENCES

1. Barnes, W. L. and J. C. Price, "Calibration of a Satellite Infrared Radiometer," Applied Optics, 19, 13 (1 July 80), pp 2153-61.

2. Sherman, Dr. Allan, NASA/GSFC, private conversation.

3. Donohoe, M. J., Internal NASA/GSFC memorandum to I. L. Goldberg (24 April, 1973).

4. Williams, Mr. Vernon, Westinghouse Electric Corp., Systems Development Division, Baltimore, MD, private communication.

5. Donohoe, M. J., A. Sherman, and Capt. D. E. Hickman, "Radiant Coolers - Theory, Flight Histories, Design Comparisons, and Future Applications." AIAA Paper No. 75-184, (1975).

6. Kruger, R., A Contamination Experiment Investigating the Failure of the Nimbus IV Filter Wedge Spectrometer, NASA-SP-298, (1972).

7. Predmore, Dr. Roamer, NASA/GSFC, private conversation.

8. McGuire, James P., Contamination from Skylab as Determined from the Solar Coronagraph Data, TM X-73353, NASA/MSFC, (Dec 1976).

9. Sheehy, Robert N., Contamination Monitor, X-713,68-134, NASA/GSFC (Jan 1968).

10. Science, "Debate Continues on Bomb That Wasn't," Vol. 209, (1 Aug 1980), pp 572-3.

11. Science, "Navy Lab Concludes the Vela Saw a Bomb," Vol. 209, (29 Aug 1980), pp 996-7.

12. Aviation Week and Space Technology, "Clandestine Nuclear Test Doubted," (11 August 1980), pp 67-72.

13. Metzger, Mr. Eric, ORI, Inc., Silver Spring, MD, (formerly of NASA/GSFC), private conversation.

14. Osantowski, Mr. John, NASA/GSFC, private conversation.

15. Linstrom, Mr. Loren, NASA/GSFC, private conversation.

16. Heaney, J. B., H. Herzig, and J. Osantowski, "Auger spectroscopic examination of MgF2 - coated Al mirrors before and after UV irradiation," Applied Optics, 16, 7, (1977), pp. 1886-1889.

17. Neupert, Dr. Werner, NASA/GSFC, private conversation.

18. Epstein, Dr. Gabriel, NASA/GFC, private conversation.

19. Mangus, Mr. John, NASA/GSFC, private conversation.

20. Fechtig, H., "In-Situ Records of Inter-Planetary Dust Particles - Methods and Results," Interplanetary Dust and Zodiacal Light, (H. Elsasser and H. Fechtig, ed) Springer Veslag, Berlin, (1976), pp. 143-157.

21. Hallgren, D. S. and C. L. Hemenway, "Analysis of Impact Craters from the S-149 Skylab Experiment," Op sit, pp. 270-74.

22. Barengoltz, J., An Estimate of Particulates in the Vicinity of a Shuttle Orbiter Due to Meteoroid Impact.

23. Kessler, D. L., P. M. Landry, B. G. Cour-Palais, and R. Taylor, "Collision Avoidance in Space," IEEE Spectrum, (June, 1980), pp. 37-41.

III. CLASSIFICATION OF CONTAMINATION RECEIVERS

3.1 OVERVIEW

This chapter provides an outline which establishes generic classes of contamination receivers. These classes were selected to provide a method by which any instrument or support subsystem can be related to its critical surface parameters. The identification of critical parameters will vary as a function of a number of variables which are discussed in the following text.

The location of a surface is important because it determines the extent to which it will be exposed to contaminants and radiation fluxes from the external environment. These fluxes are strongly dependent upon the extent of the surface's exposure to the exterior environment, its orientation with respect to the satellite's velocity vector, its orientation with respect to the sun line, etc.

In order to determine what levels of degradation are acceptable, it is necessary to consider the application. For example, instruments such as solar coronagraphs and earth limb sensors must view a weak target in close angular proximity to a strong source of background flux and are therefore more strongly degraded by stray light scattering than are similar sensors viewing celestial targets.

Specification of the spectral range is also essential because the desired properties of the underlying medium, the undesired properties of the

contaminant, and the physics of the degradation mechanism may all be highly dependent upon the wavelength (for optical and thermal radiation problems), charged particle energy (for electronic problems) or other key spectral property of the system.

The critical properties of the surfaces are those attributes whose alteration degrades the performance of the system. The definition of what constitutes a "critical" parameter may depend on factors such as the function of the surface, its spectral range, and its operating temperature. In order to quantify the analysis of contamination effects, it is necessary to identify the critical property in these terms. For example, the reflectivity of a mirror surface over a given spectral range may be specified in terms of its throughput, or specular reflectivity, and its total integrated scatter (TIS).

Operating temperature may be important for a number of reasons. In the first place, it determines which contaminants will accrete on a given surface and which will not. It may also determine whether an accreted contaminant will react chemically or whether it will remain in its original state. Finally, the operating temperature is important in determining which portion of the electromagnetic spectrum is critical in the analysis of radiative heat transfer. For example, the rejection of heat at ambient temperatures requires a high emissivity in the 10 μm spectral range while the efficient rejection of heat at 100 K requires a high emissivity in the 30 μm range.

The typical surface defines a class of materials and/or a structure which is employed on most of the surfaces under consideration. Materials may vary in tbeir sensitivity to chemical reaction with accreted contaminants, their fracture mechanism under high velocity impact, etc. The structure of a surface is important for a number of reasons. For example, the optical thickness, impact properties, chemical stability and index of refraction of typical optical coating materials may become increasingly important in the presence of contamination.

3.2 CLASSIFICATION OF CONTAMINATION RECEIVER SURFACES

3.2.1 Sensor Optical Surfaces

A. Grazing incidence mirrors

1. Location: Telescope collecting optics

2. Typical applications: Observation of sun, stars, earth's auroral activity

3. Spectral range: EUV - Soft X-ray

4. Critical property: Specular reflectivity at grazing incidence

5. Operating temperature: ambient range

6. Typical surface: Uncoated precious metal (Ir, Pt, Au)

B. Coated normal-incidence mirrors

1. Location: Collecting optics or scan mirrors

2. Typical applications: Observation of terrestrial and celestial targets

3. Spectral range: UV-visible-IR

4. Critical property: Specular reflectivity in the normal to 45° angular range

5. Operating temperature: ambient

6. Typical surface: Metal reflective surface (Al, Ag or Au) overcoated with stable transparent material MgF_2, Al_2O_3, SiO

C. Uncoated normal-incidence mirrors

1. Location: Collecting optics or scan mirrors

2. Typical Applications: Observation of earth's surface, earth's atmosphere and celestial targets

3. Spectral range: IR

4. Critical property: Specular reflectivity in the normal -45° angular range

5. Operating temperature: ambient

6. Typical Surface: Au

D. Refractive optics

1. Location: Lenses, windows, prisms, etc.

2. Typical applications: Observation of terrestrial and celestial targets, horizon sensing, star tracking

3. Spectral range: Near UV - visible - IR

4. Critical property: Refraction

5. Operating temperature: Ambient

6. Typical surface: Bulk material (quartz, MgF_2, Ge, etc.) overcoated with quarter-wave thickness of low index of refraction material

E. Cryogenic Optics

1. Location: Collecting optics in cooled telescopes

2. Typical applications: observation of celestial targets or earth's upper atmosphere

3. Spectral range: middle - far IR

4. Critical property: Specular reflectivity or refractivity

5. Opearting temperature: 2 - 200K

6. Typical surfaces: Uncoated Au mirrors and coated Ge lenses

3.2.2 Thermal Control Surfaces

A. Spacecraft Thermal Coating

1. Location: External surfaces of spacecraft

2. Typical application: Passive control of spacecraft thermal energy budget

3. Spectral range: Emissivity (ϵ) over blackbody spectrum peaked at about 10 μm; absorptance (α) over solar spectrum peaked at about 500 nm

4. Critical property: Choose α/ϵ to achieve thermal control

5. Operating temperature: Typically -10 to +50°C

6. Typical surface: Aluminum overcoated with optically transparent/IR opaque material

B. Radiant Cooler Thermal Patch

1. Location: Cold stage of radiant cooler; shielded from direct or indirect sun, earth, and spacecraft rays

2. Typical application: Maintain IR detectors at low temperatures

3. Spectral range: Thermal - far IR (10 - 100 μm)

4. Critical property: High emissivity

5. Operating temperature: 80-120K

6. Typical surface: Serrated surface coated with high emissivity material

3.2.3 Stray Light Suppression Surfaces

A. Black Baffles

1. Locations: Sun shades, annular baffles, field stops and aperture stops of sensor optics

2. Typical application: Extinction of out-of-field radiation

B. Heat Rejection Mirrors

1. Location: Field stops, aperture stops, or baffles in solar-viewing or cyrogenically-cooled telescopes

2. Typical applications: Reject out-of-field light and minimize instrument heating

3. Spectral range: UV-visible-IR

4. Critical property: Specular reflectivity

5. Operating temperature: ranges from cyrogenic to above ambient

6. Typical surfaces: Uncoated Au or overcoated Al with knife edges

C. Spectrometer Slits

1. Location: Focal plane of spectrometers

2. Typical applications: Provide spatial resolution in one dimension only

3. Spectral range: X-ray - UV - visible - IR

4. Critical property: Geometric fidelity and extinction of out-of-field light

5. Operating temperature: ranges from above ambient to cryogenic

6. Typical surface: black anodized Al with knife edges.

D. Radiant Cooler Shields

1. Location: Intermediate stages of radiant coolers

2. Typical application: Shield cold patch from radiation

3. Spectral range: Thermal - far IR if unilluminated; UV - far IR if illuminated by solar radiation (direct or indirect)

4. Critical property: Specular reflectivity

5. Operating temperature: 80-200K

6. Typical Surface: Au or Al mirrors

3.2.4 Calibration Surfaces

A. Diffuser Plates

1. Location: Exposed to sunlight and within the field-of-view of a sensor (in calibration mode)

2. Typical application: Periodically inserted into sensor's field-of-view to calibrate throughput of the entire instrument

3. Spectral range: near UV/visible/near IR

4. Critical property: Diffuse (Lambertian) reflectivity

5. Operating temperature: ambient

6. Typical surface: Aluminum, sandblasted or overcoated with TiO_2 or $BaSO_4$.

B. Blackbody Calibration Source

1. Location: Calibration system

2. Typical application: Calibrate IR channels of a sensor

3. Spectral range: IR

4. Critical property: High emissivity

5. Operating temperature: ambient to several hundred C

6. Typical surface: High emissivity material on the inner surface of a cavity.

3.2.5 Electronic Surfaces

A. Solar Cells

1. Location: Exterior surfaces of spacecraft and solar panels

2. Typical application: Power source for spacecraft

3. Spectral range: 0.3 - 1.1 μm

4. Critical property: Transmissivity of window

5. Operating temperature: ambient range

6. Typical surface: Silicon cells with transparent/ conducting contacts (Sn or In oxides) operated with SiO or with another transparent anti-reflection coating.

B. Photomultiplying and electron multiplying surfaces

1. Location: PMTs and microchannel plates

2. Typical application: detection of photons and charged particles

3. Spectral range: UV - near IR and charged particles

IV. PROPERTIES OF OPTICAL AND RADIATION CONTROL SURFACES

4.1 OVERVIEW

In general, there are five critical surface properties which must be specified for high-performance imaging optical surfaces: throughput, RMS surface figure, autocorrelation function, microroughness, and scratch/dig quality. The first property, the throughput, is specified as the reflectivity of a mirror surface or the transmissivity of a refractive surface. Throughput must also remain high in non-imaging systems such as reflective diffuser plates and transmissive solar cell windows. The other four properties relate to the quality of the image and its freedom from spurious images due to radiation not originating at the conjugate object point.

The surface figure and autocorrelation function are measures of the "macro" and "intermediate" scale of departures of the true surface from its ideal contour. The RMS surface figure error is one factor in the wavefront error budget of the system and thereby determines the sharpness of the image. Most spaceborne imaging optical systems are designed to be diffraction limited; i.e., to have an image spreading due to wavefront error which is small with respect to that produced by diffraction. The autocorrelation function is a measure of the intermediate-scale periodicity of the system. An optical surface whose autocorrelation function exhibits peaks displaced from the zero frequency will tend to act as a diffraction grating and will produce spurious images at specific wavelengths. The two remaining optical surface

parameters, microroughness and scratch/dig quality, are indices of the localized or "micro" departure of the surface from its ideal contour. These localized defects tend to produce wide-angle scattering of light by the surface. Of all the properties discussed above, loss of throughput and increase in stray light scattering are the most contamination-sensitive degradations.

The absolute levels of throughput extinction and stray light enhancement which are "acceptable" in any given optical instrument are highly mission-specific. They depend not only upon the hardware but also upon the observational target, the background flux levels, the spectral characteristics of the measurement, and the types of data which are being sought. For example, the suppression of stray light scattering is most critical in instruments which must view a weak target which has a small angular separation from a strong source of noise. (A solar coronagraph and an earth limb-viewing instrument are such instruments.) Because the level of the background radiation far exceeds that from the target, the surface quality is a great deal more critical than it would be for an identical optical system whose viewing was restricted to stellar targets. Any attempt to set an absolute limit on the stray light level of a sensor would also have to consider the details of its optical configuration.

Similar arguments can be made concerning throughput degradations. A sensor which performs absolute radiometric measurements (e.g., a solar constant monitor), will be far more sensitive to throughput changes than most instruments. Likewise, a spectrometer or a multispectral radiometer will be very sensitive to the spectral dependence of the throughput degradation. Because of the great diversity of measurement objectives and operating environments, it is impossible to define "acceptable" levels of contamination on an absolute basis.

Since absolute levels of contamination cannot be defined on a general basis, we have adopted a relative approach in which "acceptable" levels of contamination in space are defined as those whose degradation of critical

surface parameters is small in comparison to those induced by manufacturing errors and by exposure to the ambient space environment. In this chapter, we develop models which permit such intercomparisons to be made.

Contamination of an optical surface can be produced by the accretion of either a film or particulates. A molecular film which is "smooth" will change the throughput of an optical surface. Irregularities in the film due to random deposition will also increase the effective microroughness of the surface. Deposition of particulates which are significantly smaller than the operational wavelength of the sensor will also increase the microroughness of the surface, as will the impact craters of very small micrometeoroids. Deposition of particulates which are larger in comparison to the wavelength, impact craters of large micrometeroids, and scratches and digs introduced in manufacturing will also increase the stray light scattering of the surface.

In the following sections, we develop models which may be used to perform a quantitative intercomparison of these various effects. The levels of contamination to which a surface is exposed and the precise characteristics of the contaminants (such as size distribution of particulates, complex index of refraction of thin films, etc.) are subject to considerable uncertainties. Because of these problems, it is not worthwhile to use extremely complex models to obtain precise predictions of surface scattering behavior in the presence of the different contaminants. Our goal instead is to develop simple, understandable, and physically justifiable models which will permit inter-comparison of effects to within a factor of two to four.

4.2 INCREASES IN THE TOTAL INTEGRATED SCATTER (TIS) OF A MIRROR SURFACE

4.2.1 Definition and Relationship to Surface Parameters

The Total Integrated Scatter (TIS) of mirror surface is the fraction of incident radiation which is scattered in all non-specular directions. It is a dimensionless parameter and is easily related to localized surface defects by simple mathematical models in two limits: the limit in which the

surface defects are much larger than the wavelength and the limit in which they are much smaller. The intermediate case in which these two dimensions are comparable is more complex.

4.2.2 Large Defect Model

When the surface defects are much larger than the wavelength, λ, the TIS produced by large-scale surface defects is independent of wavelength and is proportional to the sum of projected areas of the defects, A, divided by the total surface area, S. By intuition, it would seem that the TIS conbritubtion of the contaminants should equal A/S. In fact, the TIS is twice this value due to diffraction-enhanced scattering by the edges of the defects.[1,2] If $(TIS)_m$ is the total integrated scatter of the uncomtaminated surface, then the TIS of the contaminated surface for normally incident light will be:

$$TIS = (TIS)_m + 2A/S \qquad (4-1)$$

This model is physically valid in the limit of geometric optics where the wavelength is small in comparison to the structural dimensions of the defect. It will be used to compare surface defects which include reflective particulates, dielectric particulates, and craters due to micrometeoroid impacts. The particulates will be modelled as cubes whose edge dimension is δ and the craters will be modelled as hemisphere of radius δ. The cubic particulate assumptions is chosen because of the cubic crystal structure of many metals and ionic compounds which are likely surface contaminants. Hemispherical surface craters are an excellent approximation to the actual contours of high velocity impact craters.[3,4,5]

Based upon these assumptions, the TIS contribution due to N cubic particulates of dimension lying "flat" on a surface of area S is:

$$TIS = 2N\delta^2/S, \qquad \delta >> \lambda \qquad (4-2)$$

If N hemispherical craters of radius are present on a surface of area S, then:

$$TIS = 2\pi N\delta^2/S, \qquad \delta >> \lambda \tag{4-3}$$

4.2.3 Small Defect Model

A different approach must be used in the limit where the wavelength of the radiation is larger than or comparable to the dimension δ, of the defects. In this regime, the height of the defects is important as well as their projected cross-sectional area. The TIS may be related to the RMS microroughness, Δ, of the surface and to the angle of incidence of the light, θ, by the equation:

$$TIS = 1 - \exp\left[-(4\pi\Delta \cos\theta)^2/\lambda^2\right] \tag{4-4}$$

In our analysis, we will assume normal incidence ($\theta = 0$) and will consider the most stringent requirements, i.e., those in which the microroughness is small with respect to wavelength. Equation 4-4 may then be approximated by its first-order Taylor series expansion:[6]

$$TIS \cong (4\pi\Delta/\lambda)^2 \qquad \Delta << \lambda \tag{4-5}$$

The microroughness Δ, or equivalent micro-roughness of various classes of surface defects will be calculated in the following section.

4.3 MICROROUGHNESS MODELS

4.3.1 Scope and Applications

The purpose of the following mathematical models is to calculate the microroughness contribution produced by several types of small-scale surface irregularities. Reflective particulates and craters in an uncoated reflective surface are considered as local perturbations to the surface height and are

accommodated directly in the microroughness model. This model may also be used with minor modifications to estimate the change in effective micro-roughness due to the accretion of dielectric particulates and due to the cratering of a refractive surface. A model of molecular desposition of an irregular dielectic film is also presented.

4.3.2 Assumptions

We assume that the uncontaminated mirror surface has an RMS microroughness, Δ, and a Gaussian distribution about the mean surface, $z = 0$. In other words, the probability that a given point on the mirror surface will have a vertical displacement z from the mean surface, takes the form of the error function with a standard deviation of Δ:[6]

$$\rho(z) = (\Delta \sqrt{2\pi})^{-1} \exp(-z^2/2\Delta^2) \qquad (4\text{-}6)$$

This surface is illustrated in Figure 4-1-A.

We now assume that a surface area, S, is randomly contaminated by a number, N, of particulates which are shaped as cubes with side dimension δ. We also assume that the coverage is sufficiently sparse so that most of the area remains uncovered by contaminant particulates, i.e., that $N\delta^2 << S$, that no particulates are stacked on top of each other, and that all of the cubic particulates are oriented with one axis along the z-direction. This model is illustrated in Figure 4-1-B.

To analyze the effect of craters in a reflective surface, we may simply use the above assumptions in an inverse form. We will first consider cubic craters to demonstrate the symmetry of this model and will then analyze a more realistic model in which hemispherical craters are treated. To model cubic craters, we assume that a surface area, S, contains N cubic craters of dimension δ, as shown in Figure 4-1-C.

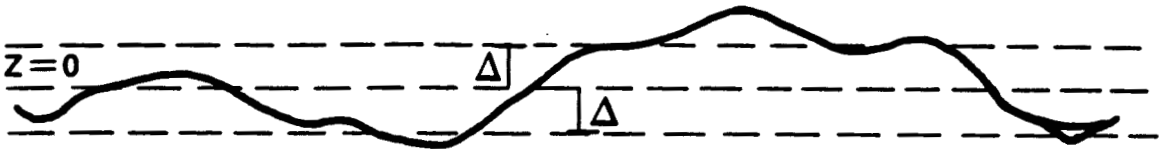

FIGURE 4-1-A. UNCONTAMINATED MIRROR SURFACE

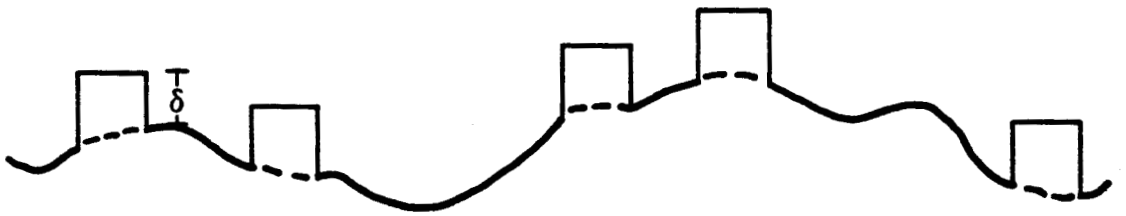

FIGURE 4-1-B. MIRROR SURFACE CONTAMINATED BY RANDOMLY-SPACED CUBIC PARTICULATES OF DIMENSION δ

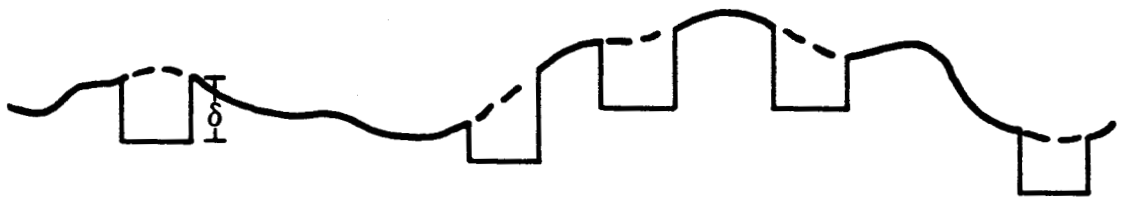

FIGURE 4-1-C. MIRROR SURFACE WITH RANDOMLY-SPACED CUBIC CRATERS OF DIMENSION δ

FIGURE 4-1. SURFACE CONTOURS FOR MICROROUGHNESS MODEL

4.3.3 Microroughness Calculation for Reflective Particulates and Craters

We now calculate Δ', the microroughness of the particulate-covered surface, by assuming that the effective surface height is increased by δ in that fraction of the total area which is covered, $N\delta^2/S$. For a cratered surface, we assume that the effective surface height is decreased by δ over an area $N\delta^2/S$.

The value of Δ' is calculated in the Appendix. From Equation A-7, we find:

$$\Delta' = \sqrt{\Delta^2 + N\delta^4/S} \qquad (4-7)$$

It is important to note that equation 4-7 produces the same result for both particulate contamination and cratering. This result is significant because it makes it possible to compare the relative magnitudes of two different degradations, particulate accretion and high velocity micrometeroid impact, without requiring any instrument-specific or mission-specific assumptions.

4.3.4 Hemispherical Crater Model

In the previous analysis, we calculated the microroughness contribution due to cubic craters. In order to make our crater model more physically realistic and consistent with the large scale defect models, we now calculate the microroughness contribution of hemispherical craters of radius δ. From equation A-11, in the Appendix, the microroughness is:

$$\Delta' = \sqrt{\Delta^2 + N\pi\delta^4/2S} \qquad (4-8)$$

4.3.5 Extension of Particulate and Cratering Models to Refractive Materials

It is straightforward to extend this model to the analysis of refractive particulate contamination and of craters in refractive optical surfaces. To do this, we simply compare the changes in optical path which are produced by the different mechanisms. A reflective cube of dimension δ on the surface of a mirror decreases the optical path of a normally-incident ray by 2δ; a refractive cube of dimension δ whose index of refraction is n increases the optical path of a normally-incident ray by $2\delta(n-1)$. Likewise, a cubic crater of depth δ in a mirror surface increases the optical path by 2δ while a crater of depth δ in a refractive mirror overcoat decreases the optical path by $2\delta(n-1)$. Because of the simple nature of these relationships and of the symmetry of positive and negative perturbations of the optical path, we may use the same analytical technique as outlined in the Appendix to derive an effective microroughness value for a mirror surface with refractive particulate coverage or with cubic craters in a refractive coating.

$$\Delta' = \sqrt{\Delta^2 + N\delta^4(n-1)^2/S} \qquad (4-9)$$

The effective microroughness for hemispherical craters in a refractive coating is:

$$\Delta' = \sqrt{\Delta^2 + N\pi(n-1)^2\delta^4/2S} \qquad (4-10)$$

4.3.6 Microroughess Calculation for Random Deposition of a Thin Film

A thin film coating can be built up on an optical surface by the random accretion of contaminant molecules. Because of the statistical nature of this process, the contaminant layer will be uneven and will contribute to effective microroughness of the surface.

To model this contamination mechanism, we assume that molecules of diameter D are deposited on the surface in a random manner to form a film of

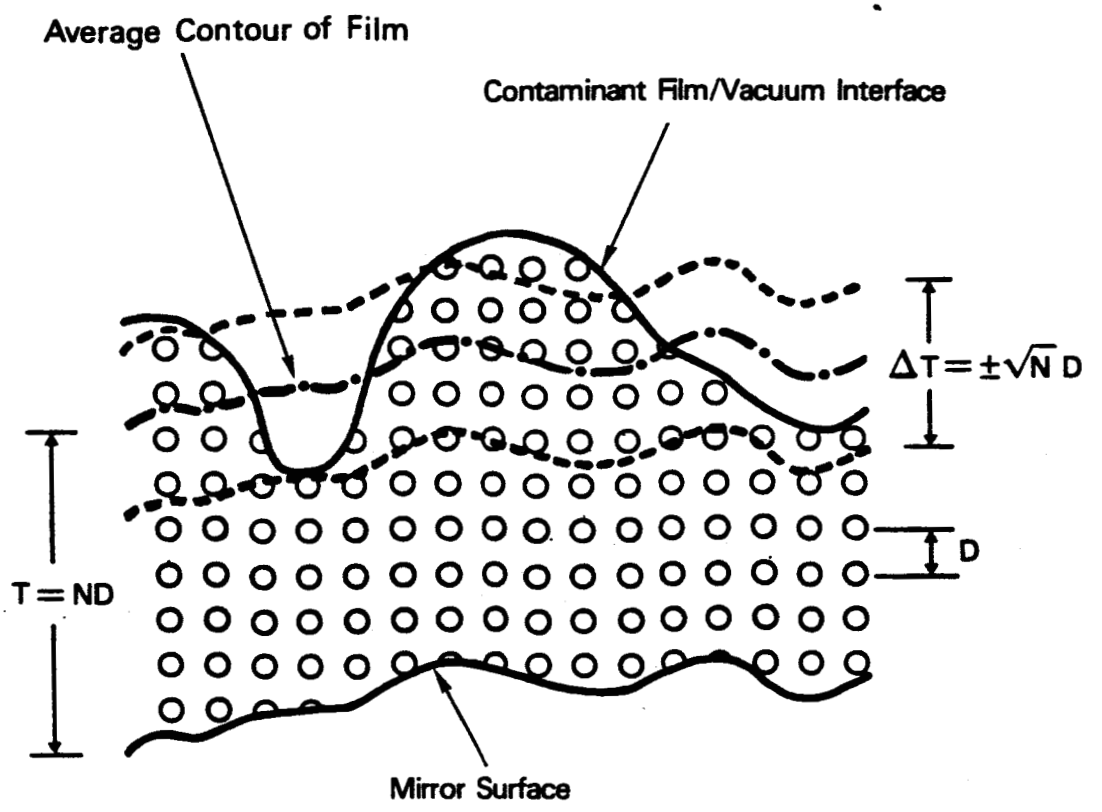

FIGURE 4-2. RANDOM DEPOSITION OF A MOLECULAR CONTAMINANT FILM

average thickness T. The average thickness may also be expressed as an average number of molecules, N:

$$N = T/D \tag{4-11}$$

The statistical variations will produce an RMS variation in the film thickness, ΔT, which is equal to the square root of N, as shown in Figure 4.2.

$$\Delta T = \pm\sqrt{N}\, D = \pm\sqrt{TD} \tag{4-12}$$

If the index of refraction of the contaminant film is n then the microroughess of the contaminated mirror will be:

$$\Delta' = \sqrt{\Delta^2 + TD(n-1)^2} \tag{4-13}$$

4.4 CALCULATION OF TOTAL INTEGRATED SCATTER PRODUCED BY SURFACE DEFECTS

4.4.1 TIS Determination

The models which were developed in the preceding section will now be used to calculate the Total Integrated Scatter (TIS). For large scale defects, it is obvious that the total TIS is the sum of the individual components. For example, if an uncontaminated mirror with a total integrated scatter of $(TIS)_m$ is degraded by large-scale particulates with a total integrated scatter of $(TIS)_p$ and by large-scale craters with a total integrated scatter of $(TIS)_c$, then the total integrated scatter of the contaminated mirror surface is:

$$TIS = (TIS)_m + (TIS)_p + (TIS)_c \tag{4-14}$$

It is also true that the TIS components produced by microroughness add linearily in the smooth surface limit. To illustrate this fact, we consider the root-sum-square relationship by which microroughness components are added. In analogy with the above example, if an uncontaminated mirror surface exhibits an RMS microroughness of Δ_m and is contaminated by small-scale particulates which produce a microroughness component Δ_p and by

small-scale craters which produce a microroughness component Δ_c, then the net microroughness, Δ, will be:

$$\Delta = \sqrt{\Delta_m^2 + \Delta_p^2 + \Delta_c^2} \tag{4-15}$$

In the smooth surface limit, equation 4-5 is a valid approximation and the TIS component produced by each surface degradation is proportional to the square of its microroughness. The following expression results:

$$TIS = TIS_m + TIS_p + TIS_c \tag{4-16}$$

We have demonstrated above that all TIS contributions add linearily whenever the approximations which have been invoked in this chapter are valid. We now compute the TIS contributions for small scale surface defects by using equation 4-5 and the appropriate microroughness model. The TIS for reflective cubic particles of dimension δ is:

$$TIS = 16\pi^2 N\delta^4/\lambda^2 S \tag{4-17}$$

The TIS for hemispherical craters of radius δ in a metal surface is:

$$TIS = 8\pi^3 N\delta^4/\lambda^2 S \tag{4-18}$$

For cubic particulates with index of refraction n, the TIS equation becomes:

$$TIS = 16\pi^2 N\delta^4 (n-1)^2/\lambda^2 S \tag{4-19}$$

Hemispherical craters in a refractive material produce a TIS which is given by the equation:

$$TIS = 8\pi^3 N\delta^4 (n-1)^2/\lambda^2 S \tag{4-20}$$

A randomly-deposited film of molecular contaminants with index of refraction n, molecular diameter D, and average film thickness T will produce a TIS contribution equal to:

$$TIS = 16\pi^2 TD(n-1)^2/\lambda^2 \qquad (4-21)$$

These TIS values which are obtained in the small-scale limit and those which were obtained in the large scale limit are summarized in Table 4-1.

4.4.2 Discussion of TIS Model Results

There are several significant implications of the TIS models which should be considered. It should be noted that the TIS is a linear function of the defect density, N/S, for all of the types of particulates and craters considered in Table 4-1. The linearity of these terms and of equations 4-14 and 4-16 is consistent with our intuition that the total scattering produced by a number of random defects should be a linear sum of the individual contributions. It is also important to realize that the TIS of large-scale defects is independent of wavelength but the TIS of small scale defects is inversely proportional to the square of the wavelength. Small scale defects become increasingly significant scatterers as the wavelength becomes shorter, but the wavelength dependent is not as strong as the inverse-fourth-power Rayleigh law for isolated small-scale scattering centers.[6] It is also important to note the fact that the TIS of large scale defects is proportional to the cross-sectional area of the defect while the TIS of small scale defects is proportional to the product of the area and the square of the height.

4.4.3 Worst-Case TIS model

In the analysis of the degradations produced by particulates, it is often illustrative to perform a "worst-case" analysis where a given volume of contaminant is assumed to be divided into particulates of uniform dimension δ, and where δ is chosen to maximize the degradation. The small-scale defect

TABLE 4.1

TIS CONTRIBUTIONS OF SURFACE IRREGULARITIES

	Defect Type	Reflective Cubic	Hemispherical Craters in metal	Dielectric Particulates	Hemispherical Craters in Dielectric	Irregular Molecular films
Defect Scale		particulate edge = δ	radius = δ	edge = δ, dielectric constant = n	radius = δ, dielectric constant = n	Thickness = T, Molecular diameter = D, Index of refraction = n
	$\delta >> \lambda$	$2N\delta^2/S$	$2\pi N\delta^2/S$	$2N\delta^2/S$	$2\pi N\delta^2/S$	------
	$\delta << \lambda$	$16\pi^2N\delta^4/\lambda^2S$	$8\pi^3N\delta^4/\lambda^2S$	$16\pi^2N\delta^4(n-1)^2/\lambda^2S$	$8\pi^3N\delta^4(n-1)^2/\lambda^2S$	$16\pi^2TD(n-1)^2/\lambda^2$

analysis indicates that the TIS of each particle is proportional to the fourth power of its linear dimension δ, and therefore that the magnitude of the TIS produced by a constant volume of particulates is linearily proportional to δ. The large scale model, on the other hand, predicts that the magnitude of the TIS produced by each particle is proportional to the square of δ and therefore that the magnitude of the TIS produced by a constant volume of particulates is inversely proportional to δ.

We assume that the small-scale model is valid for values of δ which lie below the cross-over point of these two curves and that the large-scale model is valid above this point. A worst case value of δ may be established by equating the values of the TIS predicted by the large-scale and the small-scale models, as shown in Figure 4-3. For example, we can find the worst-case value of δ for reflective cubic particulates by equating the TIS values predicted by equations 4-2 and 4-26.

$$2N\delta^2/S = 16\pi^2 N\delta^4/\lambda^2 S \qquad (4\text{-}22)$$

The worst-case value of δ which results is:

$$\delta = \lambda/\pi\sqrt{8} \qquad (4\text{-}23)$$

As we would anticipate, the value of δ which produces the worst-case degradation is of the same order of magnitude as the wavelength. It is important to realize that this model is not physically rigorous and that a complex Mie-scattering analysis is necessary to obtain accurate predictions of the scattering behavior in this regime. The worst case value of δ predicted in equation 4-23 should serve as a reasonable approximation whose error is comparable with or smaller than uncertainties in our knowledge of the particulate distribution.

A more realistic model of particulate scattering is presented in a paper by Elson, Bennett, and Bennett.[2] Experimental data have also be published.[7]

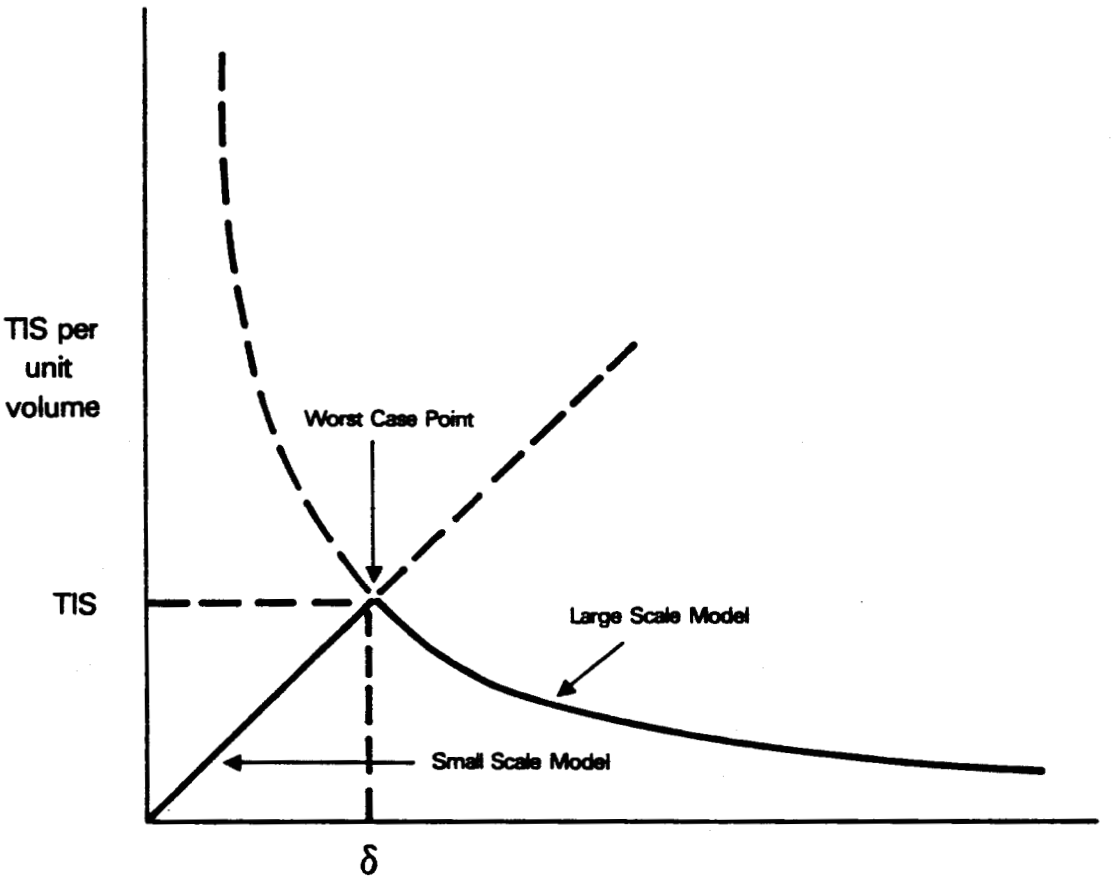

FIGURE 4-3. LINEAR PLOT OF TIS AS A FUNCTION OF δ FOR CONSTANT VOLUME OF PARTICULATES

4.5 THROUGHPUT REDUCTION DUE TO A CONTAMINANT FILM

4.5.1 Qualitative Discussion

Throughput is defined to be that fraction of the incident radiation which undergoes the "desired" interaction at the optical surface: specular reflectance for a mirror, Snell's law refraction for a lens or prism, diffuse reflection for a diffuser plate, or extinction for a blackbody surface. The remainder of this section will be restricted to the discussion of mirrors and lenses.

The analysis of the transmission or reflection which occurs at a surface is complicated if the surface is overcoated in which case one must consider the interference between components of radiation which are reflected or transmitted by each interface. With the exception of precious metals, metal reflective surfaces must be overcoated with a transparent ionic material or they will oxidize spontaneously. Aluminum, for example, has been known to oxidize in the presence of a very low partial pressure of oxygen. Uncoated silver will tarnish in the presence of trace amounts of sulfur-bearing gasses and is therefore rarely used. In fact, gold is the only reflective surface which is commonly used without an overcoat and its high reflectance spectral region is confined to the infrared and long-wave visible (red-orange) spectral region. Rhodium, platinum, and iridium may be used if an uncoated surface with high visible reflectivity is required or if high electron density is required for EUV and soft x-ray applications.

Mirrors which employ aluminum or silver as their reflective material are generally overcoated with an ionic compound. Magnesium fluoride is the most common overcoat material for spaceborne mirrors because it is chemically inert, physically strong, transparent through most of the UV, visible and IR, and has a low index of refraction (1.38 in the visible)[8]. Other overcoat materials include calcium flouride, lithium flouride (for vacuum UV work) and silicon monoxide. Coatings are used in the normal dispersion regime, i.e., their index of refraction decreases monotonically with increasing wavelength. In general, the thickness of the optical coating is selected so that the optical path difference between the light reflected from the mirror surface

and that reflected from the front surface of the overcoat is an integral number of wavelengths in the spectral region of greatest interest. Lenses and other transmitting optical elements are frequently overcoated with a low index of refraction material to enhance their throughput. Since transmissivity is the desired property on these surfaces, the coating thickness is chosen so that there is a half-wave optical path difference between the reflected components from the two interfaces, causing them to interface destructively (i.e., $\lambda/4$ coating thickness).

It is important to note two factors:

1. The optical path difference is dependent upon the angle of incidence and also upon the wavelength dependent index of refraction.

2. It is impossible to satisfy this requirement over a wide spectral range.

When the reflectance of a coated mirror is measured over a wide spectral range, it is found to exhibit reflectance maxima and minima coincident with the conditions for constructive and destructive interference between the rays reflected by the metallic surface and those reflected by the overcoat. This effect is illustrated by the solid line in Figure 4.4. An absorbing layer on the surface of the overcoat produce an "etalon effect" in which the reflectivity is strongly degraded at the reflectance minima but is relatively unaffected at the maxima. The broken line in Figure 4.4 illustrates this effect. A reflecting layer, such as the metallic film which could be deposited by a chemical release experiment, would also exhibit an interference effect. Experimental measurements have confirmed these phenomena. It has also been established that the action of vacuum UV radiation or charged particle bombardment can produce a thin film of strongly absorbing carbon or polymerized hydrocarbon on a surface contaminated by a transparent hydrocarbon material.[9,10] An uncoated mirror experiences a more wavelength-independent degradation due to the accretion of an absorbing contaminant on its surface.

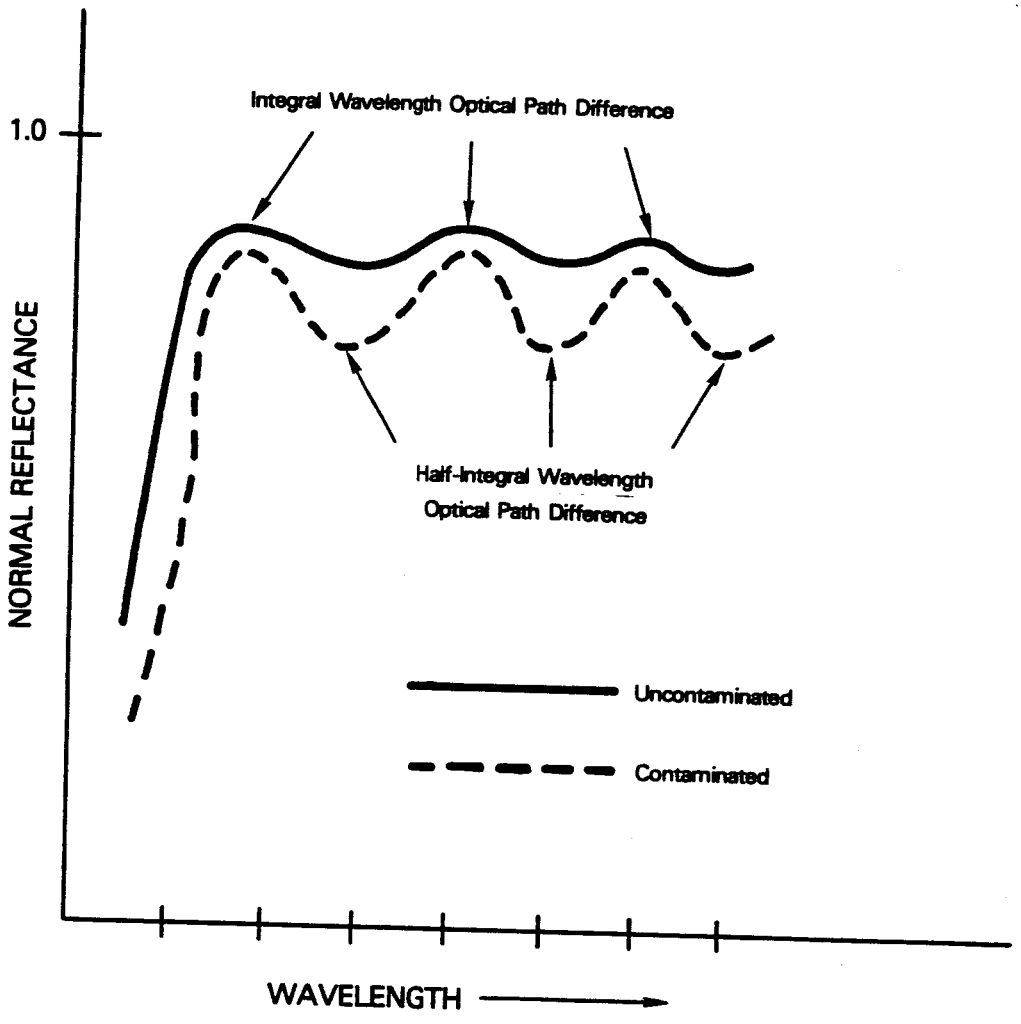

FIGURE 4-4. REFLECTANCE OF A COATED MIRROR

4.5.2 Mathematical Model of Film Contaminants

A contaminant film which is either reflective or absorptive will diminish the throughput of a transmissive optical surface; an absorptive contaminant film will also diminish the throughput of a mirror surface. A precise analysis of the throughput degradations produced by a contaminant film must consider the interference between components of the incident light which are reflected and transmitted at each interface. Calculations of throughput values may be performed by straightforward but mathematically ponderous application of electromagnetic boundary value theory.[11]

Since our goal in this analysis is to obtain a quantitative but simple relationship between film thickness and loss of throughput, we shall neglect interference effects and utilize a simple skin effect model. The first case which we consider is that of a metallic film on a refractive surface. The skin depth, s, of a metal film is defined as that depth beneath the metal surface at which the electric field strength has fallen to 1/e of its surface value. Since this attenuation is exponential, the electric field strength at a distance x from the metal surface, E(x), may be defined as a function of the field strength at the surface, E(o), and the distance x:

$$E(x) = E(o)\exp(-x/s) \tag{4-24}$$

The power, P(x), is proportional to the square of the field strength and therefore obeys the functional relationship:

$$P(x) = P(o)\exp(-2x/s) \tag{4-25}$$

If the thickness of the metal film is T and the minimum acceptable throughput is ϕ, then we have:

$$\phi = P(T)/P(o) = \exp(-2T/s) \tag{4-26}$$

The maximum acceptable film thickness becomes:

$$T = -(s \ln\phi)/2 \tag{4-27}$$

If an absorbing contaminant film is present on the surface instead of a metal film, then equation 4-27 may also be used. In this case, s is the extinction coefficient of the absorbing medium.

A reflecting film deposited on a mirror surface will not produce a large decrease in reflectivity and will therefore not be considered here. On the other hand, an absorbing film deposited on a mirror surface will alternate the incident and reflected radiation. Because the radiation undergoes two-way pass through the contaminant film, the maximum tolerable thickness is half as great as it would be on a lens:

$$T = -(s \ln\phi)/4 \qquad (4\text{-}28)$$

4.6 DECREASE IN EMISSIVITY OF A "BLACK" SURFACE

4.6.1 Discussion

Since atmospheric conduction and convection are negligible at spacecraft altitudes, radiation is the dominant mechanism by which thermal balance is maintained. Consequently, the preservation of high emissivity surfaces is necessary for the proper operation of a number of critical subsystems, including the thermal control subsystems of spacecraft and the cold patches in radiant coolers. High emissivity surfaces are also required on blackbody radiation sources and on light-estinguishing optical stops, including sun shades, aperture stops, field stops, baffles, and spectrometer slits.

4.6.2 Spectral Dependence

The amount of heat radiated by a "greybody" surface, i.e. a surface with spectrally independent emissivity, is simply proportional to the fourth power of its absolute temperature. The amount of radiant energy absorbed by such a surface is directly proportional to the magnitude of the incident radiant energy and does not depend upon its spectral distribution. Although some of the surface coatings utilized in spacecraft systems may be considered

as greybodies for practical purposes, other surfaces, by necessity or by design, exhibit very spectrally-dependent emissivities.

In general, thermal control surfaces are used for heat dissipation. To be effective, they must have high emissivities in the wavelength regime corresponding to their maximum temperature. The blackbody radiation spectrum for a surface at ambient temperature has its peak in the vicinity of 10 μm; the spectrum for a typical radiation cooler cold patch has its peak in the vicinity of 30 μm. When surfaces which operate at ambient temperatures are under consideration, it is possible to simplify the calculation of the thermally-emitted energy by using ϵ, an effective emissivity. The value of ϵ is determined by integration of the spectrally-dependent emissivity weighted in proportion to the Planck blackbody function at ambient temperature.

If the surface is exposed to an external source of radiation, it is also necessary to minimize the emissivity in the spectral range of that source. For example, thermal control surfaces which are exposed to sunlight (direct, reflected, or scattered) should have low emissivities in the near IR-visible near UV spectral range. The solar absorptance coefficient, α, is an average emissivity in this spectral range which is weighted in proportion to the intensity of the solar spectrum.

In all calculations which involve emissivity, it is necessary to specify the spectral range over which the high emissivity is required. Telescope baffles must have high emissivities throughout the spectral range of the attached instruments if they are to extinguish stray light effectively. The emissive surfaces of blackbody calibration must likewise remain "black" throughout the passbands of the infrared sensors which they calibrate.

The operating temperature of the surface is important for a number of reasons. As previously mentioned, this temperature determines the spectral region over which the high emissivity is critical. The temperature also determines which species of molecular contaminants can accrete on the surface. In some cases, the emissivity of a material can vary signficantly with temperature over a narrow passband.[12]

4.6.3 Geometric Effects

Geometry may also be a critical factor in the analysis of emissivity. It is important to realize that the emissivity of a surface can vary with angle. As a general rule, the emissivity of a surface decreases as the deviation of the incident ray from the normal angle.[12]

Concave surfaces have effective emissivities which exceed their surface emissivities. This effect occurs because some of the rays which are reflected from the surface at one point strike the surface at a second point and are absorbed there. A blackbody calibration source is generally configured as a cavity so that its effective emissivity will be as close as possible to unity. Cold patches in radiant coolers may also be configured with irregular surfaces. For example, the Thematic Mapper cold patch has a honeycomb geometry and is overcoated with a paint which is white at visible wavelength and black in the far IR. The nominal effective emissivity of the honeycomb is 0.95 and its nominal solar absorptance is 0.40.[13]

Parametric relationships between surface emissivity and effective emissivity have been developed for simple cavity geometries such as cones, cylinders, and spheres. In the computation of the effective emissivity of such a cavity, surfaces with specular and diffuse residual reflectivities produce different results.[14] In any event, the use of an irregular surface will make the cold patch less sensitive to contamination than a planar surface with an equivalent effective emissivity would be.

4.6.4 Contaminant Effects

Obviously, the contaminants which will degrade a high emissivity surface most severely are those which lower its effective emissivity. This degradation may be produced by any of the following mechanisms:

1. Accretion of a reflective metal film whose thickness is a sufficient fraction of the skin depth of that metal in the relevant spectral region

2. Accretion of a dielectric film whose index of refraction, n, is sufficiently large in the relevant spectral region to produce a substantial reflectance at its outer surface. For normal incidence, the reflectivity of the film will be $(n-1)^2/(n+1)^2$

3. The accretion of a thermally-insulating material which is opaque in the relevant spectral region and whose thermal resistance is comparable to the resistance which is present between the cold patch and the refrigerated component (e.g. the focal plane assembly of an IR sensor).

4. The accretion of enough particles to cover a signficant fraction of the surface.

5. The impact of particles at sufficiently high momentum to remove segments of the high emissivity material and expose the underlying substrate. (The creation of small craters within the high emissivity surface layer would tend to increase, rather then decrease, the emissivity and would therefore not create a problem.)

Of all the mechanisms discussed above, only the accretion of a metal film appears to be significant at low levels of contamination. Because of the concave geometry of most cold patches and of the performance margin which is built into radiant coolers, they appear to be less sensitive than reflective optics to contamination by a metallic film. Thermal control surfaces of spacecraft should also have a sufficient performance margin to withstand a greater loss of throughput than can a precision optical instrument. Because of these factors, we shall restrict our analysis of reflective films to optical sensors. If a mission specific analysis must be made of a thermal control surface, the sensor throughput models can be employed.

4.7 REFERENCES

1. Born, M. and E. Wolf, Principles of Optics, Permagon Press, Oxford, 3rd Ed., (2965), p. 659.

2. Elson, J.M., H.E., Bennett, and J.M. Bennett, "Scattering from Optical Surfaces" in Applied Optics and Optical Engineering, Vol, VII, edited by R.R. Shannon and J.C. Wyant, Academic Press, New York, (1979), p 215.

3. Kessler, D.J., P.M. Landry, B.G. Cour-Palais, and R.E. Taylor, "Collision Avoidance in Space", IEEE Spectrum, (June 1980) pp 37-41.

4. Barengoltz, J. "An Estimate of Particulates in the Vicinity of a Shuttle Orbiter Due to Meteoroid Impact", AIAA Paper No. 78-1608, (presented at AIAA/ES/ASTM 10th Space Simulation Conference, Bethesda, Md., October 1978)

5. Hallgreen, D.S. and C.L. Hermeway, "Analyais of Impact Craters from the S-149 Skylab Experiment," Interplanetary Dust and Zodiacal Light, (H. Elasser and H. Fechtig, ed.) Springer Verlay, Beslin (1976), pp 270-4.

6. Carniglia, C.K. "Scalar Scattering Theory for Multilayer Optical Coatings", Optical Engineering, Vol. 18, No. 2, (Mar/Apr 1979) pp 104-116.

7. Young, R.P., "Degradation of Low Scatter Mirrors by Particulate Contamination", AIAA Paper 75-667, (1975)

8. The Optical Encyclopedia and Dictionary, The Optical Publishing Co. Inc., Pittsfield, Mass, 25th Edition (1979), p D-74.

9. Hass, G., W.R. Hunter, "Laboratory Experiments to Study Surface Contamination and Degradation of Optical Coatings and Materials in Simulated Space Environments", Applied Optics, Vol 9, No. 9, pp 2101-10 (1970).

10. Heaney, J.B., H. Herzig, and J.F. Osantowski, "Auger Spectroscopic Examination of MgF_2-Coated Al mirrors before and after UV Irradiation", Applied Optics, Vol 16, No. 7, (July 77) pp 1886-9.

11. Haynes, D.L. and D.M. Coulson, Determination of Contamination Character of Materials in Space Technology Testing, Stanford Research Institute, SRI Project PSU-7907, (1972), pp A-1 to A-35.

12. Stierwalt, D.L. "Infrared Absorption of Optical Blacks", Optical Engineering, Vol 18, No. 2 (Mar/Apr 1979) pp 147-151

13. Thematic Mapper Conceptual Design Review Package, Hughes Aircraft Co., (July 77), pp 4-138 to 4-141.

14. Williams, C.S. and O.A. Becklund, Optics, Wiley-Interscience, New York, (1972), pp 58-62.

V. DETERMINATION OF CONTAMINATION CRITERIA

5.1 ESTABLISHMENT OF ACCEPTABLE LEVEL

The purpose of this chapter is to establish general criteria for "acceptable" levels of performance degradation due to anthropogenic contaminant sources in space such as solid fuel rocket motor firings and CRMs. Because "acceptable" is a very mission-specific term, we are forced to adopt general guidelines.

Any imaging sensor which detects electromagnetic radiation or particles has a minimum signal-to-noise ratio as one of its performance specifications. The signal is defined to be that portion of the sensor's output which is produced in response to the "desired" input, i.e., that portion of the input which originated from the proper spatial region of the target within the proper temporal window and the proper spectral band. The noise is that portion of the output which originates from all other sources, including out-of-field flux, out-of-band flux, dark currents, electronic noise, and statistical fluctuations. Each of the above error sources has several components. For example, the out-of-field flux can be attributed to diffraction, aberrations in imaging, and scattering of stray flux.

As a guideline, we shall assume that 10 percent degradation of the signal-to-noise ratio of a sensor is "acceptable". Most sensors which are designed to identify and image remote sources will have a performance margin greater than this amount. Sensors which perform absolute radiometric

measurememts can be calibrated to correct for a "one-shot" degradation, particularly when advanced notice is given, so that calibration measurements can be planned for before and after the impingement of contaminants. If this level is still not acceptable, data taking can be interrupted to permit closing of an aperture door or turning the sensor's exposed surfaces away from the contaminant source. Exposed surfaces of support subsystems which cannot be protected in this fashion (such as solar panels and thermal control surfaces) have performance margins far in excess of 10 percent.

Using these guidelines, we set 10 percent as the "acceptable" level of degradation to throughput and to any other parameter which is directly related to the signal level. Because of the multiple nature of noise sources and the root-sum-square fashion in which they are added, the absolute degradation of a single parameter of a noise-producing surface can be greater than 10 percent. We will allow the contamination-induced increase in any noise source to equal 30 percent of the value of that parameter due to other sources. For example, the TIS of a mirror surface after exposure to contamination may be as much as 130 percent of the value of the TIS due to manufacturing errors and micrometeoroid bombardment. Because of the multiple error sources, it is reasonable to expect that this level of increase in a single noise source will produce degradation in the signal-to-noise level of approximately 10 percent.

5.2 IDENTIFICATION OF WORST-CASE CONTAMINATION RECEIVER

Chapter III identifies a number of general classes of contaminant receivers. In order to specify an absolute upper limit on the envelope of avoidance for an unknown payload, we must select a worst case contamination receiver from among these classes. The worst case will be identified by a process of elimination.

Electronic surfaces, such as PMTs and high voltage sources, are generally not exposed to the external environment in a well-designed system. Langmuir probes are exposed, but are baked out at very high temperatures prior to data collection and will therefore be purged of contaminant accretions.[1] A mass spectrometer measuring the composition of the residual atmosphere would

detect spurious contributions from the contaminant, but these effects would be transient and could be identified as contaminant-induced.

A number of subsystems, such as blackbody calibration sources and radiation coolers, have surfaces which must be kept black in a given spectral passband and are therefore sensitive to the accretion of reflective contaminant films. Calibration sources are not exposed to the external environment and radiation coolers are designed with large performance margins. Both of these types of surfaces are also configured to take advantage of the "cavity effect": because of their geometry, the surface area is much larger than the aperture. A contaminant which enters the aperture will be spread over a large surface area and the effective emissivity will exceed the surface emissivity. Both of these effects tend to minimize the performance degradation produced by contaminants.

Contamination of cryogenic surfaces by material from a remote source will be insignificant in comparison to the condensation of gasses from the portions of the spacecraft which are in the immediate vicinity of the instrument. The frequently encountered problem of water vapor deposition on cryogenic surfaces was discussed in Chapter II of this report. Contamination of cryogenic surfaces by water and other condensed gasses, including NH_3, CO_2, CO, and CH_4, is discussed in the literature.[2,3,4]

Cryogenic optics are employed at infrared wavelengths; the scattering by small scale defects is therefore less severe than at visible and ultraviolet wavelengths. Because of the larger wavelengths and the problem created by internal contamination, we will not consider cryogenic infrared optics to be the most sensitive receiver of contaminants from a remote source.

Based upon the elimination of the preceding classes of contamination receivers, it appears that optical instruments which operate at visible and shorter wavelengths are the most sensitive contamination receivers. The total integrated scatter due to microroughness (Eqn. 4-5), is proportional to the inverse square of the wavelengths. It is also true that most materials absorb light strongly in the vacuum ultraviolet and all materials do in

extreme ultraviolet. In addition, the optical path of a grazing-incidence ray through a contaminant film will far exceed the film thickness. From these arguments, it would appear that grazing incidence mirrors might be the most sensitive contaminant receivers.

Experience in the operation of grazing incidence telescopes has indicated, on the contrary, that grazing incidence EUV and soft X-ray telescopes are quite insensitive to contamination (See Section 2.4.2). Some of the reasons for this insensitivity are tabulated below:

- Since the optical surface is not normal to the aperture, the distribution of contaminants on the surface will be diluted.

- Since most materials reflect to some degree at grazing incidence, a smooth contaminant film will not cause total throughput loss.

- The ability of a material to reflect EUV and soft X-ray radiation is a function of its electron density which is approximately proportional to the atomic weight of the material. Since heavy metals (Au, Pt, Ir) are used for grazing incidence mirrors, the optical distortion produced by a low-molecular weight contaminant will be small.

- Craters in the surface of a grazing incidence mirror will tend to extinguish radiation rather than scatter it.

- Grazing incidence telescopes at the current state-of-the-art do not approach diffraction-limited performance.

The types of surfaces which have been eliminated from consideration as "worst case contaminant receivers" are summarized in Table 5.1.

Because of this process of elimination, we are left with normal incidence optical instruments as worst-case contaminant receivers. Among these, vacuum UV wavelengths are the most sensitive to scattering. Sensitivity to throughput degradation is most critical at wavelengths where the skin depth is small.

TABLE 5.1
RATIONALE FOR EXCLUSION OF SURFACES FROM
THE WORST-CASE CATEGORY

Surface Type	Rationale for Exclusion
PMT, high voltage electronics	Not exposed to external contaminant flux
Langmuir probes	Baked out to remove contaminants
Mass spectrometers	Transient phenomena
Blackbody calibrators	• Not exposed to contaminant flux • Cavity geometry reduced contamination sensitivity
Radiant coolers	• Designed with large performance margin • Cavity geometry reduces contamination sensitivity • External contamination is insignificant in comparison to local contamination

TABLE 5.1 (Cont)

Cryogenic optics	• External contamination is insignificant in comparison to local contamination • IR wavelengths scatter less from small-scale defects
Grazing-incidence optics	• Geometric dilution of contaminant deposition • All materials tend to reflect at grazing incidence • Contaminants have lower optical density than mirror • Craters extinguish radiation • Diffraction-limited performance not required

5.3 DETERMINATION OF ALLOWABLE LEVELS OF CONTAMINANT FILMS

We will now find the tolerable thickness of metallic and absorbing films on optical surfaces. High-conductivity metals have small skin depths and therefore are good candidates for the worst-case contaminant on a transmissive surface. At infrared and longer wavelengths, metals obey the classical skin effect relationships and its skin depth decreases monotonically with decreasing wavelength. At visible and shorter wavelengths, the frequency of the radiation is sufficiently high that the drag forces on the electrons become significant, and the simple skin effect model is no longer appropriate.[5] Aluminum is the metal with the highest conductivity to density ratio and is also a good optical reflector. It has a skin depth which reaches a minimum of approximately 15 nanometers in the near infrared and visible regions of the electromagnetic spectrum.[6]

We now calculate the maximum acceptable film thickness, T, from Equation 4-27, by assuming that a 10 percent throughput loss is allowable, and that the skin depth, s, is 15 nanometers. ϕ is therefore equal to 0.9 and T becomes

$$T = -(1.5 \times 10^{-8}\text{m})(\ln 0.9)/2 \qquad (5\text{-}1)$$
$$= 7.9 \text{ Å}$$

Experimental reflectance data for a mirror overcoated with SiO and a 20 Å film of carbon shows a reflectance loss of approximately 20 percent at several minima coinciding with the interference minima of the uncontaminated mirror.[7] This result implies that a 10 Å film of carbon (i.e. 20 Å along the optical path) will produce a reflectance loss of approximately 10 percent.

In both of the above analyses, a contaminant film whose thickness is approximately 8-10 Å is the maximum allowable. Aluminum and carbon are very likely the worst-case examples of reflecting and absorbing contaminant films. Because these films are very thin, the scattering produced by random variations in their thickness will be negligible (see Section 4.3.6.) This effect will only be important for relatively transparent films or for reflective films on a mirror surface.

5.4 MICROMETEOROID FLUX MODEL

The micrometeoroid background in space, as discussed in Section 2.6, spans a very broad spectrum of size distributions. The craters produced by impact of these micrometeoroids will also have a broad spectrum of sizes ranging from small to large in comparison to the wavelengths of interest. To analyze the effects which micrometeoroids will produce upon a surface, we will approximate the micrometeoroid flux by a two component model:

"Small" component: 3×10^{-15} gm particles at one per second per m^2

"Large" component: 10^{-7} gm particles at 3×10^{-5} per second per m^2

These values were extracted from the Skylab data, which had assumed that the radius of the crater, δ, was three times greater than the radius of the micrometeoroid, γ. The value of γ can be calculated from the mass, m, and the density, ρ, of the micrometeoroid.

$$\gamma = (3m/4\pi\rho)^{1/3} \tag{5-2}$$

It follows that:

$$\delta = 3(3m/4\pi\rho)^{1/3} \tag{5-3}$$

If we assume a density of 5 gm/cm^3, then the flux levels become:

Small component: $\delta = 1.6 \times 10^{-5}$cm

One particle/sec-m^2

Large component: $\delta = 5.1 \times 10^{-3}$cm

3×10^{-5} particles/sec-m^2

Assuming a bombardment time of five years, we find:

Small component: $\delta = 1.6 \times 10^{-7}$ m

$$N/S = 1.6 \times 10^{8} \text{ craters/m}^2$$

Large component: $\delta = 5.1 \times 10^{-5}$ m

$$N/S = 4.7 \times 10^{3} \text{ craters/m}^2$$

We will now use this model to predict "worst case" degradations of optical surfaces. Since stray light scattering becomes more severe at short wavelengths, we will use the wavelength of 1200 Å as a sample value. This spectral region is of considerable interest in astronomy and solar physics because of the Lyman- α line of hydrogen at 1216 Å. It is also an approximate lower limit on the low-loss transmissivity of refractive materials which are used for lenses and for mirror overcoats.

The microroughness model of equation 4-8 is used to predict the TIS component created by bombardment by the small component of the flux. The microroughness is:

$$\Delta = (N\pi\delta^4/2S)^{1/2} = 4.1\text{Å} \qquad (5\text{-}4)$$

The TIS for a 1200 Å wavelength is derived from equation 4-5:

$$TIS = (4\pi\Delta/\lambda)^2 = 1.8 \times 10^{-3} \qquad (5\text{-}5)$$

The TIS produced by the larger component is computed from the area coverage mode, as in equation 4-3:

$$TIS = 2(N/S)\pi\delta^2 = 7.7 \times 10^{-5} \qquad (5\text{-}6)$$

We will now use this model to get an acceptable threshold for reflective particulate contamination under worst case conditions. We will assume a high quality, superpolished mirror surface with a microroughness of 10 Å. The TIS_m due to manufacturing errors is therefore:

$$TIS_m = (4\pi \times 10^{-9}m/1.2x10^{-7}m)^2$$
$$= 1.1x10^{-2} \qquad (5\text{-}7)$$

If we add TIS components due to micrometeoroids as specified in equations 5-4 and 5-5 to the TIS produced by manufacturing error, we obtain:

$$TIS = 1.3x10^{-2} \qquad (5\text{-}8)$$

5.5 COMPUTATION OF TOLERABLE PARTICULATE LEVELS IN WORST-CASE SCENARIO

The maximum acceptable TIS component due to particulate contamination is 30 percent of the value in equation 5-8.

$$(TIS)_p = 3.9x10^{-3} \qquad (5\text{-}9)$$

To compute the tolerable concentration of reflective particulates, we set this number equal to the TIS as defined in equation 4-22 with δ as defined in equation 4-23.

$$N\lambda^2/4\pi^2 S = 3.9x10^{-3} \qquad (5\text{-}10)$$

Using $\lambda = 1200Å = 1.20X10^{-7}m$, we may solve for N/S, the tolerable number of particles per unit surface areas, and for δ, the dimension of the particles. The surface density of particles is:

$$N/S = 4\pi^2(3.9x10^{-3})(/1.2x10^{-7}m)^2 \qquad (5\text{-}11)$$
$$= 1.1x10^{13} \text{ particles } /m^2$$

The linear dimension of the particulates is:

$$\delta = 1.20x10^{-7} \text{ m}/\pi\sqrt{8} = 1.35x10^{-8}m \qquad (5\text{-}12)$$

The total volume of particulate matter distributed on a surface area of one square meter is:

$$V = N\delta^3 = 1.1\times10^{13}\ (1.35\times10^{-8}m)^3$$
$$= 2.7\times10^{-11}\ m^3 \qquad (5\text{-}13)$$

Note that if this material were uniformly distributed over the surface, it would have an average coverage of approximately one-tenth of a monolayer and its impacts on the throughput and the stray light scattering would both be negligible. We therefore conclude that contamination by particles whose linear dimensions are approximately ten times smaller than the wavelength represents the worst case situation for a constant volume of contaminant.

5.6 DISCUSSION

It is important to realize that a total integrated scatter of 1.3×10^{-2}, as specified in equation 5-8, is a very severe requirement for a vacuum ultraviolet mirror. The analysis presented in this report assumes state-of-the-art manufacturing tolerances and neglects ground-based contamination. It further assumes that the surface in question is normal to the velocity of the contaminant-particles and is totally unshielded.

In order to minimize instrument-specific assumptions, we have neglected scattering from aperture stops, baffle edges, and other optical elements. It should be noted that any instrument which has a central obscuration, such as an on-axis reflecting telescope, could not approach the TIS value assumed here. The assumption that all the contaminant is dispersed in uniform cubic particles of the worst-case dimension is unphysical.

Because of the compound application of worst-case assumptions, we have created a very severe criterion for contamination tolerance. A more realistic model of the particulate size distribution should be used in the analysis of an actual thruster firing or CRM experiment.

5.7 STELLAR VUV OPTICS

We will now consider the same type of surface, a VUV mirror, operating in a stellar telescope. In this operational environment, the telescope views a small number of point sources and is therefore not usually performance limited by stray light scattering.[8,9] The throughput of the primary mirror would be degraded deposition of an absorbing film. As indicated in Section 5.3, carbon is probably the worst-case absorber and the tolerable thickness of a carbon film is ten Angstroms.

Particulates may also degrade the throughput of a VUV mirror by scattering light in non-specular directions. We may calculate the tolerance for particulate contamination by using the approach outlined in Section 5.5 of this report. The values of λ and δ remain the same; the maximum tolerable TIS is ten percent.

The tolerable density of particles is:

$$N/S = 4\pi^2(0.1)/(1.2\times10^{-7}m)^2 \qquad (5\text{-}14)$$
$$= 2.7\times10^{14} \text{ particles/m}^2$$

The total volume of particulate matter distributed on a surface area of one square meter is:

$$V = (2.7\times10^{14})(1.35\times10^{-8}m)^3 \qquad (5\text{-}15)$$
$$= 6.6\times10^{-10}m^3$$

Thus scattering by small particulates can produce significant throughput loss in the vacuum ultraviolet spectral region. Visible and infrared telescopes will be less sensitive to contamination by small particulates.

5.8 CONTAMINATION OF SOLAR CELLS

Solar cells are used to provide electrical power for virtually all earth-orbiting civilian satellites and for most military satellites as well.

These solar cells are the most sensitive contamination receivers on a large class of satellites which do not carry optical sensors or other sensitive payload instruments (communication satellites, for example). Solar cells are therefore the logical components to analyze in order to determine the maximum contamination tolerance of satellites.

The characteristics of solar cells are outlined briefly in Section 3.2.5.B of this report. The transmissivity of solar cell surfaces is degraded by either absorbing or reflecting contaminant films. The cells are photo-active in the spectral region from 0.3 to 1.1 μm and achieve their maximum efficiency in the near-infrared and visible portions of this passband. This spectral region coincides with the skin depth minimum of aluminum, causing the cells to be very sensitive to degradation by deposition of an aluminum film. From the analysis contained in Section 5.3 of this report, we may conclude that an aluminum film eight Angstroms thick will produce a transmissivity degradation of approximately ten percent. Tolerances for other metal films and absorbing films may be computed from equation 4-27.

Solar cells are non-imaging devices and are therefore not degraded by distortions of the optical wavefront. They are sensitive to degradation by particulates if these particulates cover an appreciable fraction of the surface area and absorb or back-scatter the incident light. As a rough approximation, we may assume that half of the light is backscattered (and lost) while the other half is scattered in the forward direction and reaches the silicon. The throughput, ϕ, is then related to the TIS by the following expression:

$$\phi = 1 - TIS/2 \qquad (5\text{-}16)$$

This approximation is justifiable for particulates which are small with respect to the wavelength. Particles which are large with respect to the wavelength scatter predominantly in the forward direction if they are dielectric and in the backward direction if they are metallic.[10]

From equation 5-16, we find that a TIS of 20Å corresponds to a throughput loss of ten percent. A wavelength of 7000 Å may be used to characterize the solar cell spectrum for wavelength-dependent calculations. By substituting this value into equation 4-23, we obtain a worst-case value for the particulate dimension.

$$\delta = 7\text{x}10^{-7}\text{m}/\pi\sqrt{8} = 7.9\text{x}10^{-8}\text{m} \qquad (5\text{-}17)$$

To compute the maximum tolerable concentration of particulates, we set the TIS equal to 0.2, use the above value for δ, and solve equation 4-2 for the ratio N/S.

$$\begin{aligned} N/S &= 0.2/2(7.9\text{x}10^{-8}\text{m})^2 \\ &= 1.6\text{x}10^{13}\ \text{particles/m}^2 \end{aligned} \qquad (5\text{-}18)$$

The total volume of particulate matter distributed on a surface area of one square meter is:

$$\begin{aligned} V &= N\delta^3 = (1.6\text{x}10^{13})(7.9\text{x}10^{-8}\text{m})^3 \\ &= 7.9\text{x}10^{-9}\text{m}^3 \end{aligned} \qquad (5\text{-}19)$$

If this material were distributed uniformly over the surface, it would have a thickness of 79 Angstroms, i.e., ten times greater than that of the maximum tolerable aluminum film.

5.9 REFERENCES

1. Sing, Mr. Milton, NASA/GSFC, Private conversation.

2. Pipes, J. G., F. G. Sherrell, B. E. Wood, and W. L. Clark, "Cryocooled Optics and Contamination," Optical Engineering, Vol. 18, No. 6, (Nov/Dec 1979), pp. 620-25.

3. Ress, E. B. and N. J. Pugel, SIRE Contamination Study, MCR-79-633, Martin Marietta Aerospace, Denver, CO, (Prepared for Hughes Aircraft Co. under Contract No. P. O. 04-409831-SC9). (Oct. 15, 1979), pp. 5-34.

4. Scialdone, J. J., Assessment of Shuttle Payloads Gaseous Environment, NASA Technical Memorandum 80286, NASA/GSFC, (May 1979).

5. Rossi, B., Optics, Addison-Wesley Publishing Company, Inc., Reading, Mass., (1965), p. 411.

6. Hayes, A. L. and D. M. Coulson, Determination of Contamination Characteristics of Materials in Space Technology Testing, Stanford Research Institute, SRI Project PSU-7907, (August 1972), p. A-10.

7. Hass, G. and W. R. Hunter, "Laboratory Experiments to Study Surface Contamination and Degradation of Optical Coatings and Materials in Simulated Space Environments," Applied Optics, Vol. 9, No. 9, (Sept. 1970), pp. Z101-110.

8. Stecker, Dr. Ted, NASA/GSFC, private conversation.

9. Code, Dr. Arthur, Univ. of Wisconsin, private conversation.

10. Elson, J. M., H. E. Bennett, and J. M. Bennett, "Scattering from Optical Surfaces" in Applied Optics and Optical Engineering (R. R. Shannon and J. C. Wyant, ed.), Academic Press, New York, (1979), p. 215.

VI. CONCLUSIONS AND RECOMMENDATIONS

6.1 SUMMARY

In this report, we have surveyed and analyzed many case histories of contamination in space and have also summarized data on the background micrometeoroid flux. Using this information, we established generic classes of contamination receivers and identified their key surface parameters. We then developed simple but quantitative models of optical throughput (reflectance of a mirror) and total integrated scatter which allowed us to compare the effects of particulate accretion, film accretion, cratering and intrinsic manufacturing defects in optical surfaces. These models produce quantitative comparisons of the various contamination effects and intrinsic manufacturing errors.

Based upon these models, we identified vacuum ultraviolet (VUV) optics as the worst-case class of contamination receiver and particulates with dimensions of approximately one-tenth wavelength as worst-case contaminants on a constant volume basis. These worst-case conditions are only applicable to instruments such as solar coronographs whose performance is limited by stray light. Particulates can also limit the throughput of stellar telescopes by scattering energy out of the beam.

Stellar VUV telescopes were found to be at least twenty times less sensitive to particulates than solar-viewing telescopes. A carbon film approximately ten Angstroms thick will produce a 10 percent throughput

degradation loss in either telescope. This factor is particularly critical for mirror surfaces which are illuminated by solar flux because transparent hydrocarbons can be altered to produce a carbon film by the action of VUV radiation. Solar cells are sensitive to throughput degradations by either metallic or absorbing films. The thickness tolerance for an aluminum film is eight Angstroms; the tolerance for a carbon film is forty Angstroms (because the solar cell is a broad-band device and because the light passes through the film on a window only once, not twice as on a mirror). It is a non-imaging device which it operates at visible and near infrared wavelengths, and is therefore relatively insensitive to particulate contamination.

The contamination tolerance of critical surfaces are summarized in Figure 6-1; the most significant findings of this report are summarized in Table 6.1.

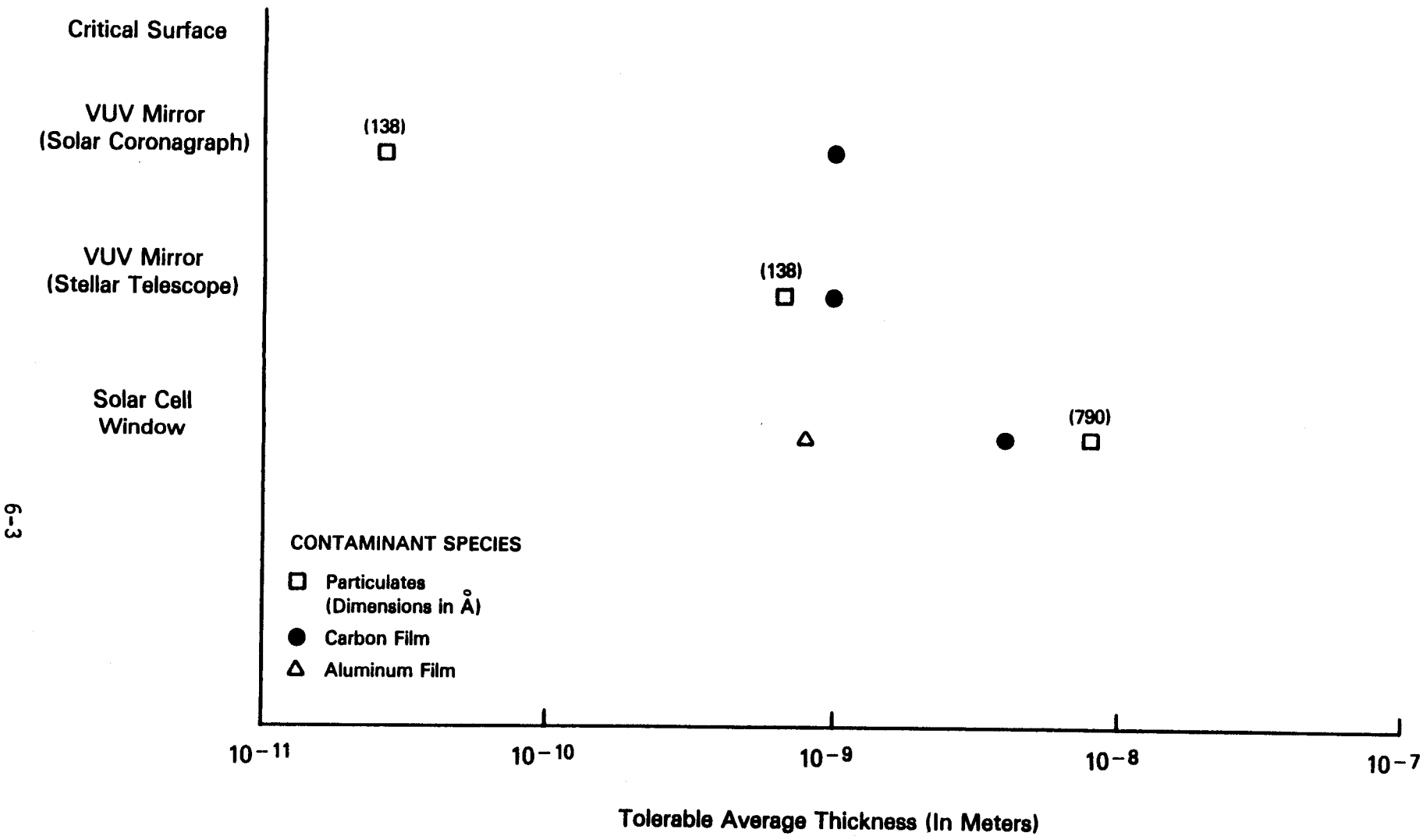

FIGURE 6-1 CONTAMINATION TOLERANCES OF CRITICAL SURFACES

TABLE 6.1

SUMMARY OF MOST SIGNIFICANT FINDINGS

1. Data from space experiments are not adequate to permit formulation of contamination criteria.

2. Contamination of cryogenic surfaces by water vapor is a common problem.

3. Hydrocarbon contaminants which are transparent on the ground may become strongly absorbing upon exposure to the space environment.

4. Critical surfaces of instruments and support subsystems may be identified and their key parameters may be specified in a generic classification scheme.

5. Simple but quantitative models of optical surface properties, including throughput and total integrated scatter, permit quantitative intercomparison of several types of surface defects.

6. Normal incidence vacuum UV optical surfaces appear to be the most sensitive contamination receivers.

7. The surface degradations produced by micrometeoroid bombardment are small in comparison to intrinsic manufacturing defects.

8. Particulates with dimensions of about one-tenth wavelength are the worst-case contaminants for vacuum UV surfaces.

9. A vacuum UV surface whose performance is stray-light limited is at least twenty times more sensitive to particulate contamination than one whose performance is throughput-limited.

10. Solar cells are sensitive to metallic film contamination and relatively insensitive to particulate contamination.

6.2 RECOMMENDATIONS FOR FURTHER STUDY

There are several problem areas which lie outside the scope of this report but which have a direct bearing upon the contamination problem. ORI recommends that all of these areas be addressed in the analysis of any contamination problem.

6.2.1 Study the Effect of Contamination During Ground Based Handling

Experience has shown that contaminant films of hydrocarbons, which are deposited on optical surfaces during ground-based handling and testing can be transformed from transparent to strongly absorbing materials in the space environment. Dust particles can also accrete on a surface, even in a clean room environment.

It is important to detect and remove these contaminants. Transparent contaminant films may be detected by ellipsometry. Particulates may be detected by an increase in the scattered light level. Florescence may also be used to detect contaminants. It would be desirable to investigate these and other methods of detecting contaminants which are not detected by visual inspection. It would also be desirable to quantify the effects of surface contamination by using the models developed in Chapter IV of this report.

6.2.2 Model the Secondary Effects of Micrometeoroid Bombardment

The analysis of micrometeoroid bombardment presented in this report considered only the primary effect: cratering of an optical surface due to direct impingement of the micrometeroid. This effect should be dominant for craters whose dimensions are small with respect to the wavelength. In the other limit, where the craters are larger in comparison to the wavelength, the secondary effect of many small particles of spacecraft material may exceed the primary effect. The secondary fragments can lower instrument performance by accretion on the sensitive instrument surfaces or by moving through the field of view of a sensor at low velocity. In the latter case, the particles will emit infrared radiation and will scatter solar radiation if they are illuminated.

6.2.3 Develop More Realistic Models of Particulate Deposition and Scattering

The worst-case particulates, as identified in this study, are those whose linear dimension, δ, is equal to $\lambda/\pi\sqrt{8}$. This value lies in the region where the small scale model, which assumes that $\delta << \lambda$, may not be valid. A more rigorous Mie scattering model should be applied if highly accurate results are required. It does appear, however, that the small particles are more injurious on a constant-volume basis than are the particles which produce resonant Mie scattering.

The worst-case model also assumes that all the particles produced by a contamination source have a value of δ equal to $\lambda/\pi\sqrt{8}$. This highly unphysical model should be replaced by a realistic particulate size distribution in order to obtain a more realistic estimate of the worst-case degradation produced by any particular upper stage or CRM.

APPENDIX

CALCULATION OF THE MICROROUGHNESS OF A CONTAMINATED SURFACE

A.1 CUBIC PARTICULATE/CRATER MODEL

We may calculate Δ', the microroughness of the particulate-covered surface, by assuming that the effective surface height is increased by δ in that fraction of the total area which is covered, $N\delta^2/S$. For a cratered surface, we assume that the effective surface height is decreased by δ over an area $N\delta^2/S$. (See Figure 4-1).

The value of Δ' may be calculated from the expression[1]

$$(\Delta')^2 = \bar{z}^2 - (\bar{z})^2 \qquad \text{(A-1)}$$

The following equations may be used to treat both the particulate contamination problem and the cratering problem. Whenever the $\pm$ symbol is used in the following equations, the plus sign refers to the particulate problem and the minus sign refers to the cratering problem.

The value of $\overline{z^2}$ is

$$z^2 = N\delta^2/S \int_{-\infty}^{\infty} (z \pm \delta)^2 \rho(z)\, dz + (1 - N\delta^2/S) \int_{-\infty}^{\infty} z^2 \rho(z) dz \quad \text{(A-2)}$$

which becomes

$$\overline{z^2} = \Delta^2 + N\delta^4/S \quad \text{(A-3)}$$

The average value of z is

$$z = N\delta^2/S \int_{-\infty}^{\infty} (z \pm \delta) \rho(z) dz + (1-N\delta^2/S) \int_{-\infty}^{\infty} z\rho(z) dz \quad \text{(A-4)}$$

which becomes

$$z = \pm N\delta^3/S \quad \text{(A-5)}$$

Combining equations A-1, A-3, and A-5, we obtain

$$(\Delta')^2 = \overline{\Delta^2} + N\delta^4/S\ (1-N\delta^2/S) \quad \text{(A-6)}$$

Recalling our previous assumption that the fractional coverage is small, we may neglect the last term in the above equation and estimate the microroughness of the contaminated surface as:

$$\Delta' = \sqrt{\Delta^2 + N\delta^4/S} \quad \text{(A-7)}$$

It is important to note that Equation A-7 produces the same result for both particulate contamination and cratering.

A.2 HEMISPHERICAL CRATER MODEL

In the previous analysis, we calculated the microroughness contribution due to cubic craters. In order to make our crater model more physically realistic and consistent with the large scale defect models, we now calculate the microroughness contribution of hemispherical craters of radius δ.

$$\overline{z^2} = N/S \int_{-\infty}^{\infty} \rho(z) \left[\int_{r=0}^{\delta} (z - \sqrt{\delta^2 - r^2})^2 \, 2\pi \, r dr \right] dz$$

$$+(1-N\pi\delta^2/S) \int_{-\infty}^{\infty} z^2 \, \rho(z) dZ \qquad \text{(A-8)}$$

By expanding the squared term inside the r integral and cancelling like terms we obtain:

$$\overline{z^2} = \int_{-\infty}^{\infty} z^2 \, \rho(z) dz - 2N/S \left[\int_{-\infty}^{\infty} \rho(z) \, z dz \right] \left[\int_{r=0}^{\delta} \sqrt{\delta^2 - r^2} \, 2\pi r dr \right]$$

$$+\frac{N}{S} \left[\int_{-\infty}^{\infty} \rho(z) \, dz \right] \left[\int_{r=0}^{\delta} (\delta^2 - r^2) \, 2\pi r dr \right] \qquad \text{(A-9)}$$

Because $p(z)$ is an even function of z, the integral of $p(z)z$ vanishes and this equation becomes:

$$\bar{z^2} = \Delta^2 + N\pi\delta^4/2S \qquad \text{(A-10)}$$

Once again, we assume that the area of crater coverage is small in comparison with the total surface area of the mirror and use the approximation:

$$\Delta' \cong \sqrt{z^2} = \sqrt{\Delta^2 + N\pi\delta^4/2S} \qquad \text{(A-11)}$$

A.3 REFERENCE

1. Reif, F., Fundamentals of Statistical and Thermal Physics, McGraw Hill, New York, New York (1965), p. 13.

1. Report No.	2. Government Accession No.	3. Recipient's Catalog No.

4. Title and Subtitle
Analysis of Contamination Effects on Critical Surfaces of Spaceborne Payloads

5. Report Date
January, 1981

6. Performing Organization Code

8. Performing Organization Report No.
TR No. 1837

7. Author(s)
James C. Bremer

10. Work Unit No. (TRAIS)

9. Performing Organization Name and Address
ORI, Inc.
1400 Spring Street
Silver Spring, MD 20910

11. Contract or Grant No.
NAS5-25607, Mod. 25

13. Type of Report and Period Covered
Final Report
11 June '80 - 12 Jan '81

12. Sponsoring Agency Name and Address
Goddard Space Flight Center
Greenbelt, MD 20771

14. Sponsoring Agency Code
NASA/GSFC

15. Supplementary Notes

16. Abstract

Contamination mechanisms such as particulate accretion, molecular film accretion, and impact cratering can degrade the quality of an optical surface by decreasing its throughput (transmissivity or reflectivity) and/or by increasing its total integrated scatter (TIS). The sensitivity of a spaceborne optical sensor to a given contaminant species depends upon a number of factors, including the spectral passband of the sensor, the type of surface (mirror or lens, coated or uncoated, etc.), the relative intensities of signal and stray light, and the desired output of the system. A precise analysis of an instrument's contamination sensitivity must consider all of these factors. It is possible, however, to define "acceptable" levels of contamination as those which produce small throughput and TIS degradations in comparison to manufacturing defects and unavoidable environmental conditions such as micrometeoroid bombardment. Solar cells and several generic classes of spaceborne instruments are analyzed by these criteria, which may be used to calculate a conservative value for the minimum separation between a spacecraft and a contamination source such as a solid fuel rocket motor or a chemical release module.

17. Key Words	18. Distribution Statement
Contamination, Spacecraft, Optics, Total Integrated Scatter, Throughput, Particulates	Unlimited

19. Security Classif. (of this report)	20. Security Classif. (of this page)	21. No. of Pages	22. Price
Unclassified	Unclassified		